iScience

CellPress
OPEN ACCESS

Article

Differential recruitment of ventral pallidal e-types by behaviorally salient stimuli during Pavlovian conditioning

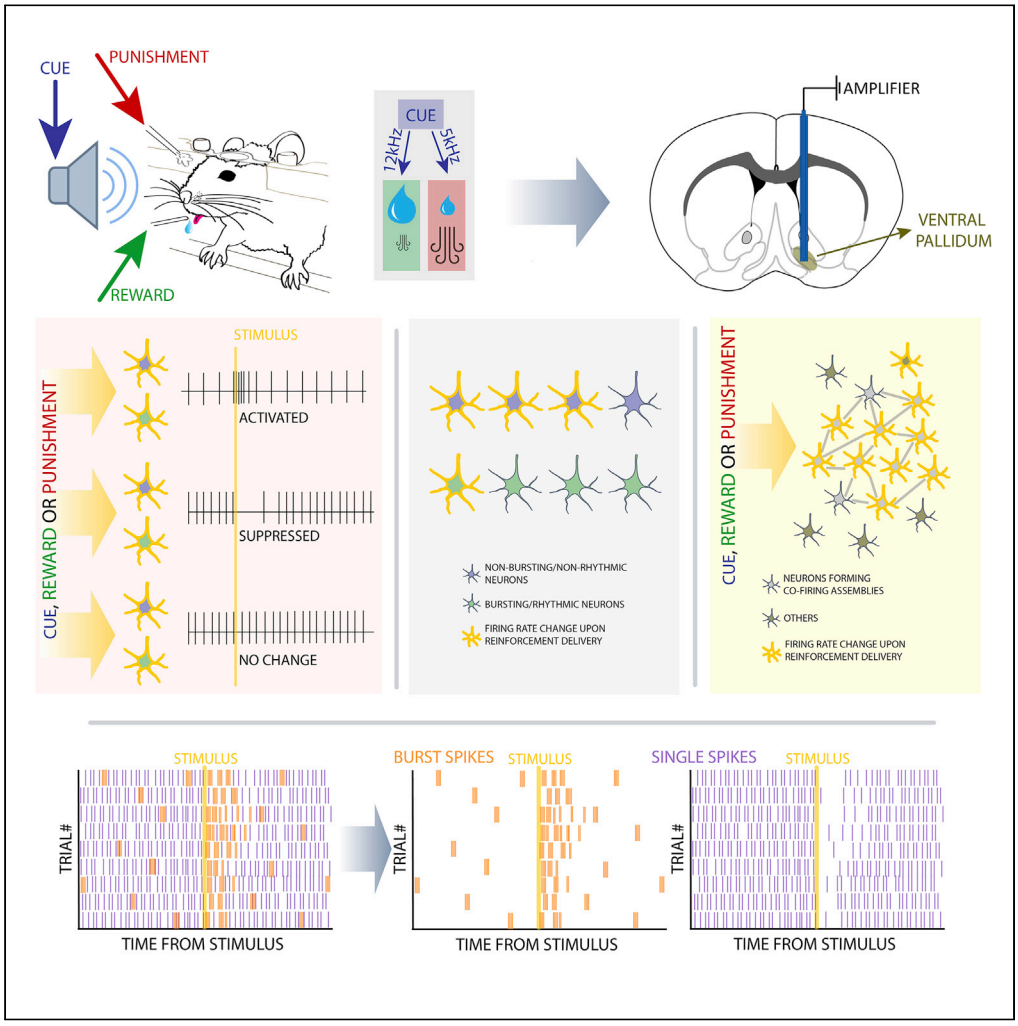

Panna Hegedüs, Julia Heckenast, Balázs Hangya

hangya.balazs@koki.hu

Highlights

VP neurons are sensitive to reward, punishment, and expectation during conditioning

Non-bursting, non-rhythmic VP neurons respond more often to salient events

VP neurons form synchronously firing assemblies responsive to reinforcement

Multiplexed single spike and burst codes were found in the VP

Hegedüs et al., iScience 24, 102377
April 23, 2021
https://doi.org/10.1016/j.isci.2021.102377

iScience

CellPress
OPEN ACCESS

Article

Differential recruitment of ventral pallidal e-types by behaviorally salient stimuli during Pavlovian conditioning

Panna Hegedüs,[1,2] Julia Heckenast,[1] and Balázs Hangya[1,3,*]

SUMMARY

The ventral pallidum (VP) is interfacing striatopallidal and limbic circuits, conveying information about salience and valence crucial to adjusting behavior. However, how VP neuron populations with distinct electrophysiological properties (e-types) represent these variables is not fully understood. Therefore, we trained mice on probabilistic Pavlovian conditioning while recording the activity of VP neurons. Many VP neurons responded to punishment (54%), reward (48%), and outcome-predicting auditory stimuli (32%), increasingly differentiating distinct outcome probabilities through learning. We identified e-types based on the presence of bursts or fast rhythmic discharges and found that non-bursting, non-rhythmic neurons were the most sensitive to reward and punishment. Some neurons exhibited distinct responses of their bursts and single spikes, suggesting a multiplexed coding scheme in the VP. Finally, we demonstrate synchronously firing neuron assemblies, particularly responsive to reinforcing stimuli. These results suggest that electrophysiologically defined e-types of the VP differentially participate in transmitting reinforcement signals during learning.

INTRODUCTION

The ventral pallidum (VP) serves as an interface between the limbic system and other structures, integrating cortical, amygdala, basal ganglia, and neuromodulatory input (Root et al., 2015; Záborszky and Cullinan, 1992). On the effector side, its projections to the thalamus, cortex, basal ganglia, and other subcortical structures including hypothalamus, ventral tegmental area (VTA), and lateral habenula (LHb) influence motivation, reinforcement learning, and attention (Faget et al., 2018; Ito and Doya, 2009; Maurice et al., 1997; Richard et al., 2016; Root et al., 2015; Smith et al., 2009; Stephenson-Jones et al., 2020; Zahm et al., 1996). Specifically, crucial aspects of VP activity in associative learning have been revealed recently, showing VP neurons encoding incentive salience and valence as well as mounting behavioral response to environmental changes (Avila and Lin, 2014; Richard et al., 2016; Stephenson-Jones et al., 2020; Tindell, 2004; Tindell et al., 2006).

How are different types of information encoded by the VP? Whether they are routed through different lines of this intricate switch board, labeled by markers such as parvalbumin, the vesicular glutamate transporter VGluT2, or the inhibitory marker GAD2 has been explored recently (Faget et al., 2018; Knowland et al., 2017; Prasad et al., 2020; Stephenson-Jones et al., 2020; Wulff et al., 2019). However, another exciting possibility is that integrating and multiplexing is also represented by different coding schemes including elements of rate and temporal code, such as characteristic firing patterns like bursts or single spike firing, rhythmic discharges, network level synchrony, and asynchronous activity (Ascoli et al., 2008; Gouwens et al., 2019; de Vries et al., 2020). Accordingly, Avila and Lin suggest that electrophysiological characterization that goes beyond the broad categories of inhibitory and excitatory cell types will enable a better understanding of how VP performs its functions (Avila and Lin, 2014).

To address the aforementioned question, we recorded VP neurons while mice performed a probabilistic Pavlovian conditioning task. By using auto- and cross-correlation techniques, we uncovered the presence of separate fast rhythmic, bursting, and non-bursting-non-rhythmic neurons, similar to previous electrophysiological categorization of VP neurons (Pang et al., 1998). We found that reinforcement-related signals were most frequent in the non-bursting, non-rhythmic population. The analysis of synchronous discharges

[1]Lendület Laboratory of Systems Neuroscience, Institute of Experimental Medicine, Budapest 1083, Hungary

[2]János Szentágothai Doctoral School of Neurosciences, Semmelweis University, Budapest 1085, Hungary

[3]Lead contact

*Correspondence: hangya.balazs@koki.hu

https://doi.org/10.1016/j.isci.2021.102377

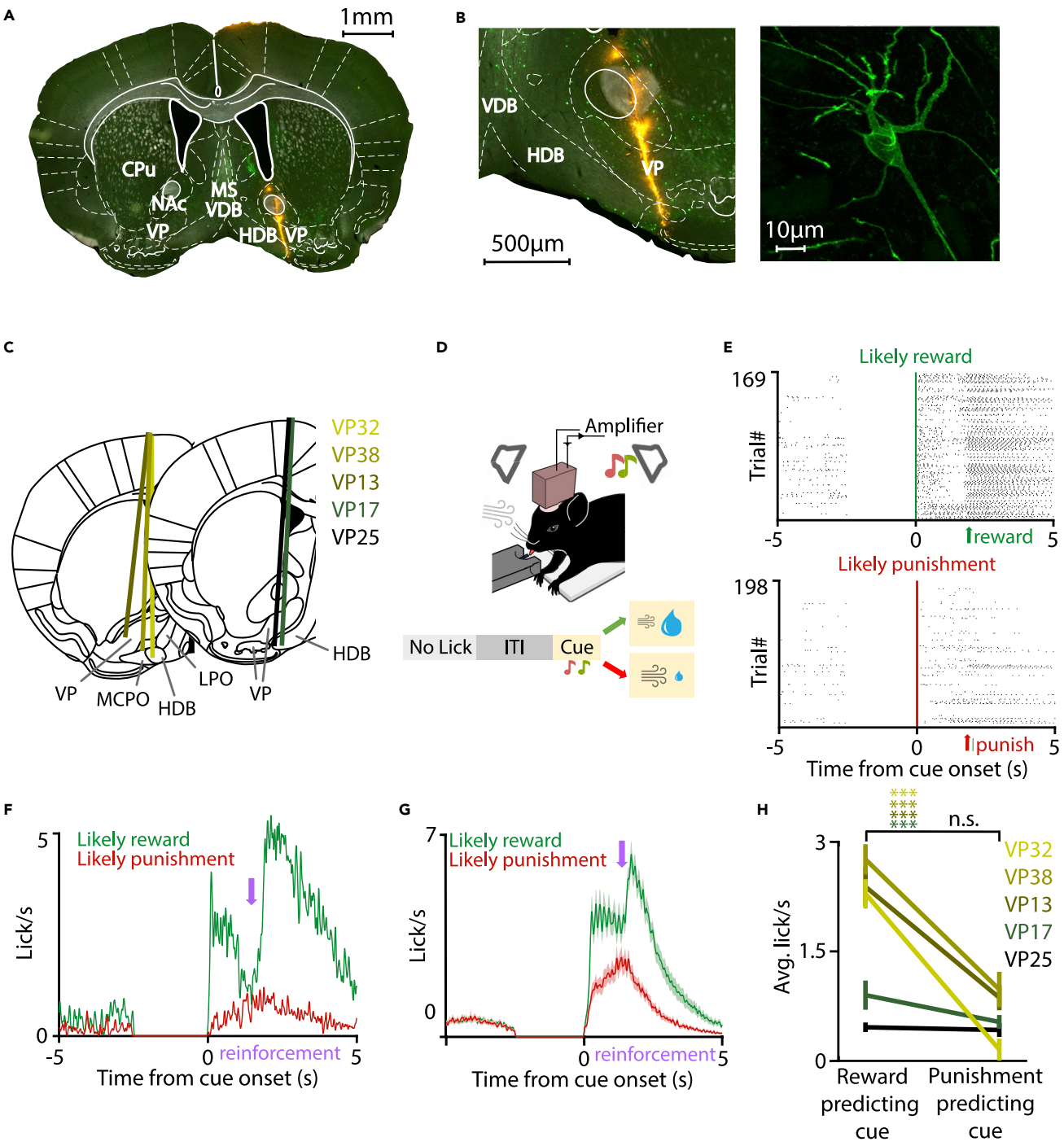

Figure 1. Targeting VP in mice performing auditory Pavlovian conditioning

(A) Coronal section from a ChAT-Cre mouse showing the tetrode tracks (DiI, yellow; ChAT+, green) through the VP. The tetrodes were advanced 0–100 µm between recording days. Although the images show the full extent of the electrode tracks, only those sessions that were conducted strictly within VP boundaries based on post hoc histological reconstruction (see transparent methods) were included. Scale bar, 1 mm.

(B) Left, magnified view of the target area. Scale bar, 500 µm. Right, confocal image of a cholinergic neuron located near the electrode track (20× magnification, z stack of 8 planes, maximal intensity projection). Scale bar, 10 µm.

(C) Reconstructed location of the electrode tracks. Only neurons recorded inside the VP were included (see transparent methods, histology).

(D) Top, schematic of the auditory Pavlovian task setup. Bottom, trial structure with possible outcomes. After the mouse stopped collecting the previous reward ("no lick"), a variable inter-trial interval started, signaled by turning an light-emitting diode off, in which no licking was allowed. Then two cue tones of well-separated pitch predicted likely reward or likely punishment.

Figure 1. *Continued*

(E) Raster plots of licking activity in an example session of one mouse. The cue predicting likely reward (top, green) elicited stronger anticipatory licking than the cue that signaled likely punishment (bottom, red).

(F) Peri-event time histograms (PETH) of licking activity from the same session. Purple arrow indicates average reinforcement delivery time (note that reinforcement time was randomized between 400 and 600 ms after cue offset according to a uniform distribution to prevent full temporal predictability of reinforcement delivery).

(G) Average licking activity (PETH) of N = 5 mice shows stronger anticipatory licking after the cue that predicted likely reward (green). Data are represented as mean ± SEM.

(H) The reward-predicting cue elicited significantly more licks in 4/5 mice. Data are represented as median ±SE of median. ***$p < 0.001$, Wilcoxon signed rank test. CPu, caudate putamen; HDB, horizontal nucleus of the diagonal band of Broca; MS, medial septum; NAc, nucleus accumbens; VDB, vertical nucleus of the diagonal band of Broca.

revealed the presence of co-firing neuron assemblies. Cells that participated in these synchronously firing assemblies showed increased responsiveness to reinforcers. Thus, VP neurons with distinct discharge types ("e-types") both at the individual and network level, likely corresponding to different coding strategies, show differences in their representation of behaviorally salient stimuli. Even within single neurons, burst and single spike firing could strongly dissociate, suggesting the presence of a distinct burst code in the VP (Kepecs and Lisman, 2003; Kepecs et al., 2002).

RESULTS

Ventral pallidal neurons are sensitive to reward, punishment, and expectation during Pavlovian conditioning

To test how different VP neurons represent behaviorally relevant events during classical associative learning, we trained mice (N = 5) on a probabilistic auditory Pavlovian conditioning task and monitored the activity of VP neurons (n = 704) (Figures 1A–1C). Mice were water restricted and head-fixed for training, listening to two pure tones of different pitch, where one tone predicted likely water reward (80% reward, 10% punishment, 10% omission) and the other tone predicted likely punishment (25% reward, 65% punishment, 10% omission; Figure 1D). Mice learned to discriminate the cue tones, indicated by differential licking activity after cue onset in anticipation of reward (Figures 1E–1G). Four of five animals showed significant behavioral discrimination at the individual level (Figure 1H).

During the task, 66% VP neurons showed phasic, short latency activation or inhibition after at least one type of behaviorally salient stimuli of the task, that is, reward, punishment, and/or the reinforcement-predicting cues (Figures 2A–2F). Around 32% (n = 222/704) of the neurons were modulated by the cues, 48% (n = 339/704) by reward, and 54% (n = 348/646, neurons recorded early in training could not be tested; Mann-Whitney U test, $p < 0.001$) by punishment (Figures 2G–2L). The majority of significantly responsive neurons showed activation, with a smaller fraction of inhibited cells (activated by cue, 148/222, 67%; reward, 253/339, 75%; punishment, 267/348, 77%). Moreover, the fraction of neurons responding to cue, reward, or punishment tended to correlate with the anticipatory lick rate difference of the animals during the task (Figures S1A–S1C). Interestingly, there was a difference in the latency of peak activation or inhibition across responses to cue, reward, or punishment. VP neurons responded the fastest to punishment, intermediate to reward, and slowest to outcome-predictive sensory cues (Figures 2M–2N).

We found that neural responses to reinforcement of opposite valence were often correlated. For instance, in 222/646 neurons, the same neuron responded with increased firing rate to both the positive and negative reinforcer. Similarly, 70/646 neurons showed firing rate decrease after both reward and punishment (Figure 2O). In contrast, only n = 3/646 neurons showed opposite responses to reward and punishment. Additionally, a large fraction of neurons showed correlated responses to reward-predictive cues and primary reward (n = 109/646 activation and n = 35/646 inhibition to both, respectively). We have found a strong co-occurrence of activation to all behaviorally salient events including cue, reward, and punishment (n = 98/646).

Given that responses to water and air-puff were often correlated, we considered whether air-puff responses could be more related to a lack of reward than the aversive quality of the air-puff. We found this was unlikely, because (1) we had shown that air-puffs were consistently avoided by mice in an operant paradigm (Figure 2C in Hangya et al. [2015]) trained in our setup (Solari et al., 2018), (2) air-puffs were accompanied by different auditory input compared with water reward rendering sensory response generalization unlikely (Figure S2A), and (3) little evidence was found for reward omission responses in the VP (Figures S2B and S2C).

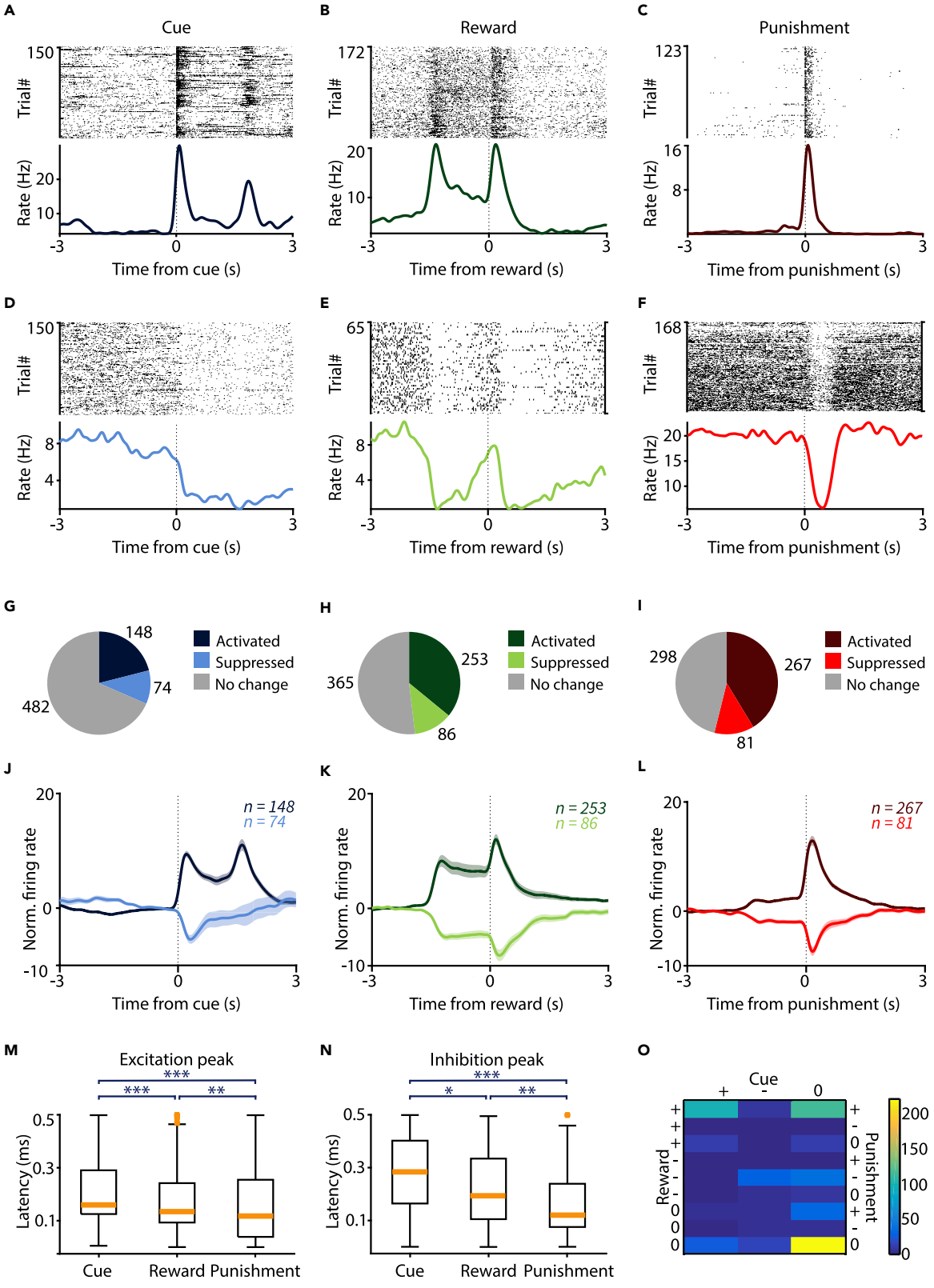
A
Cue
Trial#
Rate (Hz)
Time from cue (s)
B
Reward
Time from reward (s)
C
Punishment
Time from punishment (s)
D
E
F
G
148
74
482
Activated
Suppressed
No change
H
253
86
365
I
267
81
298
J
n = 148
n = 74
Norm. firing rate
K
n = 253
n = 86
L
n = 267
n = 81
M
Excitation peak
Latency (ms)
Cue
Reward
Punishment
N
Inhibition peak
O
Cue
Reward
Punishment

Figure 2. Ventral pallidal neurons are modulated by reward, punishment, and outcome-predictive cues during Pavlovian conditioning

(A–F) Example single VP neurons activated by cue stimuli (A), reward (B) or punishment (C), or inhibited by cue (D), reward (E), or punishment (F). Top, spike raster; bottom, PETH aligned to the respective behavioral events.

(G–I) Pie charts showing the number of all VP neurons activated and inhibited by cue (G), reward (H), and punishment (I), pooled across mice.

(J–L) Average *Z*-scored PETH of all recorded VP neurons modulated by cue (J), reward (K), or punishment (L), tested separately for the three events. Data are represented as mean ± SEM.

(M) Excitatory response latencies to predictive cues, reward, and punishment. Box-whisker plots show median, interquartile range, non-outlier range, and outliers. $^{**}p < 0.01$; $^{***}p < 0.001$, Mann-Whitney U test.

(N) Inhibitory response latencies to predictive cues, reward, and punishment. Box-whisker plots show median, interquartile range, non-outlier range, and outliers. $^{*}p < 0.05$; $^{**}p < 0.01$, $^{***}p < 0.001$, Mann-Whitney U test.

(O) Number of neurons showing different combinations of all possible responses to cues and reinforcers. +, activation; -, suppression; 0, no significant firing rate change. For instance, the color in line 1, column 1 indicates the number of neurons that were activated by all three salient events tested (cue, reward, punishment); color in line 2, column 2 indicates the number of neurons that were activated after reward but inhibited both after sound cues and punishment. See also Figures S1 and S2.

In sum, VP neurons showed an array of responses to behaviorally salient events. The fastest and most prevalent response pattern was a rapid activation after punishment. Direction of firing rate modulation was correlated across behaviorally relevant events, suggesting salience coding by individual VP neurons.

The probabilistic nature of the Pavlovian task meant that different cues were followed by reward, punishment, or omission with different (but fixed) contingencies. Mice learned these contingencies (Figure 1), which required integration of positive and negative outcomes over many trials. Based on the predictive auditory cues we played before the reinforcement, reward and punishment could be either expected or surprising according to task contingencies. This allowed us to compare VP neuronal responses with expected versus surprising outcomes.

We found that VP neurons strongly differentiated the distinct predictive cues, showing larger responses to cues that predicted likely reward (Figures 3A and 3B), reminiscent of prediction error coding (Kim et al., 2020; Schultz et al., 1997). This differential activity was more prominent in VP neurons recorded from mice that exhibited stronger behavioral discrimination of the predictive cues (Figure S3). Although reinforcement error models predict a smaller response to expected compared with surprising reward, we did not observe a significant difference (Figures 3C–3F). This might be due to the relatively small percentage of true reward prediction error-coding VP neurons that might prevent the detection of potentially small expectation-driven differences of reward responses. These results are consistent with a hypothesized role of the VP in signaling incentive salience (Ahrens et al., 2016, 2018; Tindell et al., 2005) and partially support recent findings indicating prediction error coding in the VP (Ottenheimer et al., 2020).

Non-bursting, non-rhythmic VP neurons are more often recruited by behaviorally salient events

Burst coding of salient events has emerged as a general scheme for subcortical representations: burst responses to behavioral reinforcement and reward-predictive stimuli has been demonstrated for the VTA (Schultz et al., 1997), striatum, basal forebrain (Hangya et al., 2015; Lin and Nicolelis, 2008), and LHb (Yang et al., 2018). To test whether this principle generalizes to the VP, we categorized VP neurons as bursting and non-bursting based on short-latency (<10 ms) peaks in their spike autocorrelations, indicating preferential firing with short inter-spike intervals characteristic of bursts (Laszlovszky et al., 2020; Royer et al., 2012) (Figure 4A; transparent methods).

We found that about half of VP neurons (n = 367/701, 52%; 3 neurons firing <100 spikes excluded from this analysis) fired bursts, whereas the remaining neurons were categorized as non-bursting (n = 334/701, 48%, Figure 4B). Next, we tested whether bursting neurons were more responsive to reward, punishment, and reward-predictive cues in Pavlovian conditioning. Surprisingly, we found that a larger fraction of non-bursting VP neurons showed significant responses to reinforcement (chi-square test, $p = 1.64 \times 10^{-5}$ and $p = 1.01 \times 10^{-5}$ for reward and punishment, respectively, Figures 4C–4I). This was consistent for both reward and punishment, with a higher number of non-bursting neurons showing either firing rate increase or decrease. We did not find any difference regarding the fraction of cue-responsive neurons (chi-square test, p = 0.1121). These findings were largely consistent across animals included in the experiment (Figure S4) and did not depend on the interspike interval cutoff used for defining bursts in extracellular recordings (Figure S5). Response magnitudes were variable across neurons; we provide balanced averages in

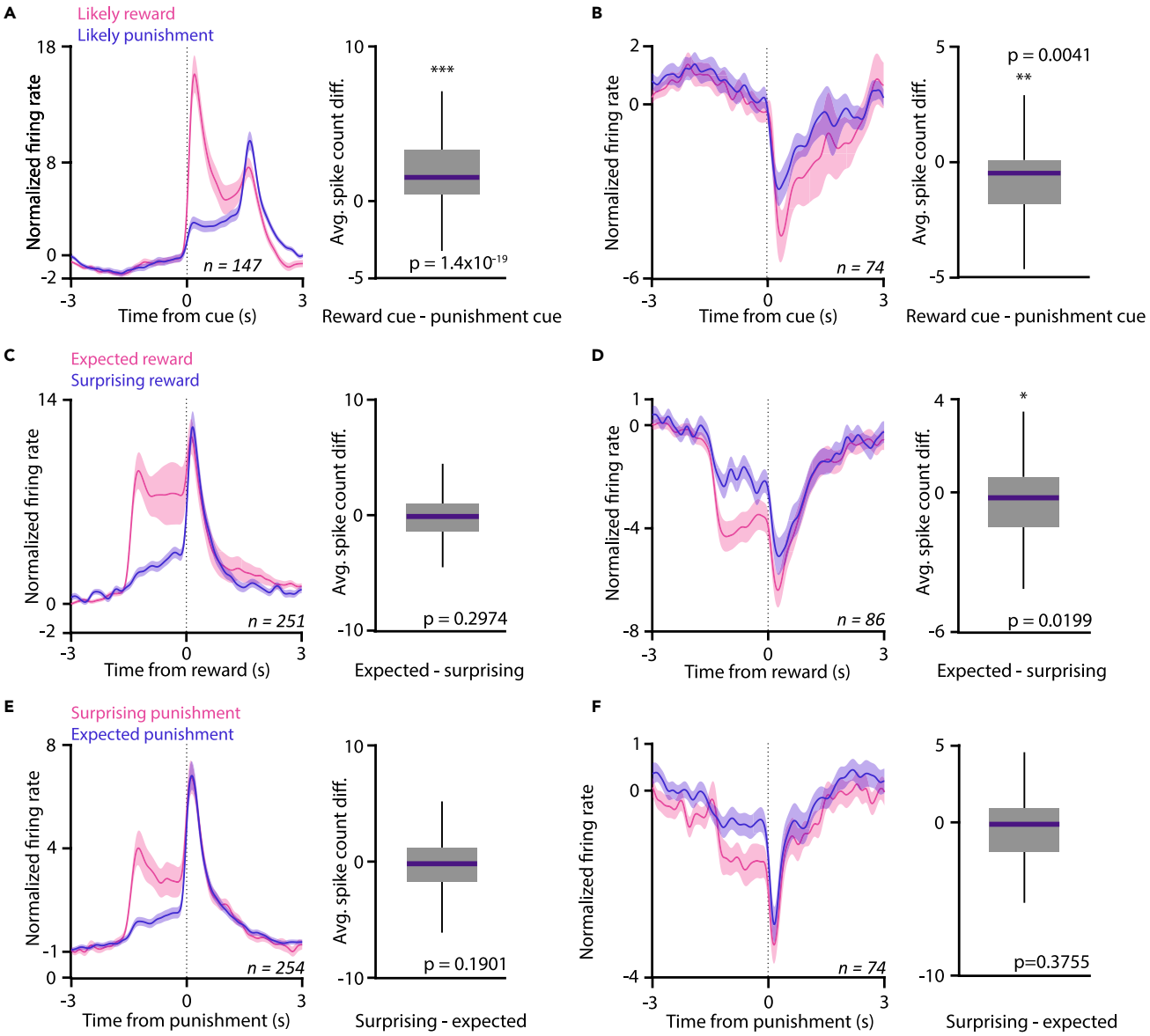

Figure 3. Ventral pallidal neurons are modulated by expectation

(A) Left, average PETH of cue-activated VP neurons after cues predicting likely reward (pink) or likely punishment (purple). Right, box-whisker plot of average spike count difference between the two outcome probability conditions in VP neurons activated by cue presentations. Data are represented as mean ± SEM. ***p < 0.001, Wilcoxon signed rank test.

(B) Average PETH and spike count difference for VP neurons inhibited after cue presentations. Data are represented as mean ± SEM. **p < 0.01, Wilcoxon signed rank test.

(C and D) Same as in (A and B), but showing responses to reward presentations. Left, reward-activated VP neurons; right, reward-suppressed VP neurons. Pink, expected reward (reward delivery after the likely reward cue); purple, surprising reward (reward delivery after the likely punishment cue). Data are represented as mean ± SEM. *p < 0.05, Wilcoxon signed rank test.

(E and F) Same as in (A and B), but showing responses to punishment presentations. Left, punishment-activated VP neurons; right, punishment-suppressed VP neurons. Pink, surprising punishment (punishment delivery after the likely reward cue); purple, expected punishment (punishment delivery after the likely punishment cue). Data are represented as mean ± SEM. Recordings with less than 5 trials in either of the tested conditions were excluded. Box-whisker pots show median, interquartile range, and non-outlier range in all panels.

See also Figures S1 and S2. See also Figure S1 and S2.

Figures 4D–4I; however, *Z* score normalization conceals response magnitude variations in these plots. We directly compared response magnitudes across bursting and non-bursting neurons and found that activation after predictive cues or punishment was significantly larger in non-bursting neurons at a conservative

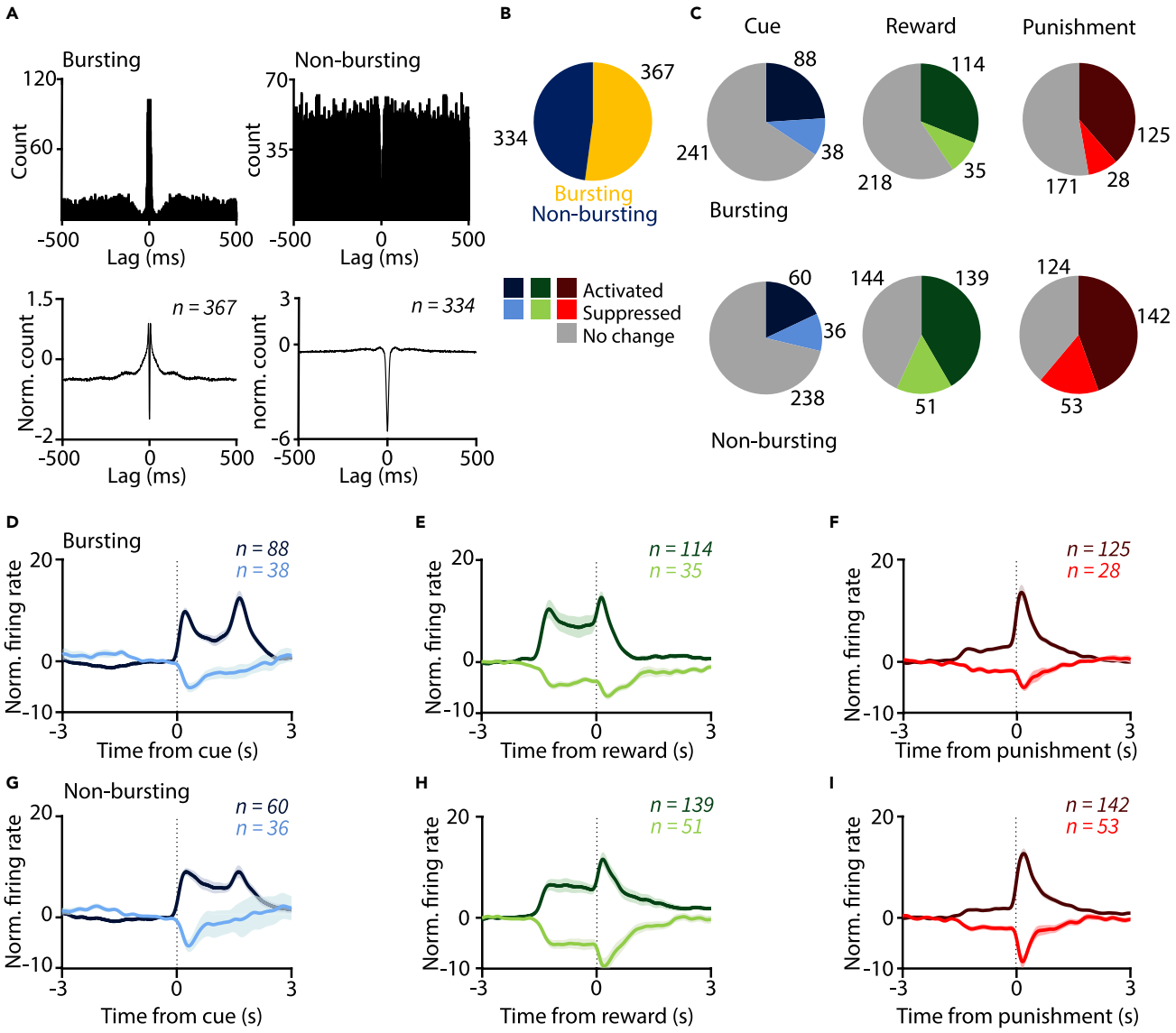

Figure 4. Non-bursting ventral pallidal neurons respond to reinforcers more frequently

(A) Top, Example autocorrelograms of a single bursting and a non-bursting VP neuron. Bottom, average across all bursting and non-bursting neurons recorded from the VP.

(B) Pie chart showing the proportion of bursting and non-bursting neurons, pooled across mice.

(C) Pie charts showing the number of all bursting and non-bursting VP neurons activated and inhibited by cue, reward, or punishment.

(D–I) Average, *Z*-scored PETHs of bursting (D–F) and non-bursting (G–I) VP neurons aligned to cue (D and G), reward (E and H), and punishment (F and I). Data are represented as mean ± SEM.

See also Figures S4–S6.

$p < 0.01$ significance threshold ($p = 0.005$ and $p = 0.001$, respectively; Mann-Whitney U-test). In addition, activation or inhibition following reward and inhibition after punishment were marginally larger in non-bursters ($p = 0.017$, $p = 0.053$, $p = 0.014$, respectively; Mann-Whitney U test). Non-bursting neurons also showed higher baseline firing rates (Figure S6A).

Based on rhythmic modulation of their autocorrelation functions, we detected a small subset of rhythmically firing VP neurons (n = 40/704, 6%; Figures 5A and 5B). We estimated the frequency at which these neurons were oscillating by their autocorrelation peak location and found that they fell in the beta/gamma range (6 beta-rhythmic and 34 gamma-rhythmic neurons were detected; see transparent methods). These

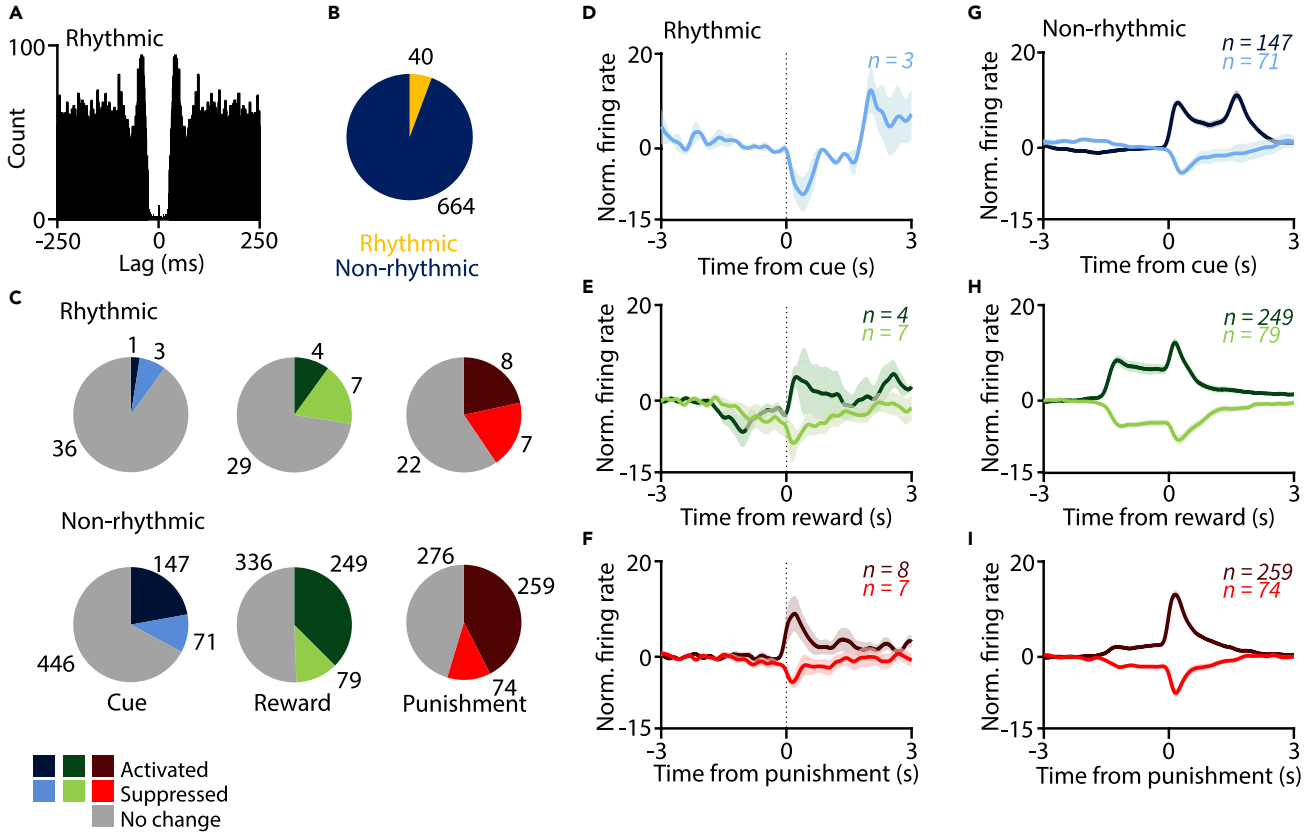

Figure 5. Salient events mostly recruit non-rhythmic neurons

(A) Example autocorrelogram of a rhythmically firing neuron.

(B) Pie chart showing the proportion of rhythmic and non-rhythmic neurons, pooled across mice.

(C) Pie charts showing the number of rhythmic and non-rhythmic VP neurons activated or inhibited by cue, reward, or punishment, pooled across mice.

(D–I) Average, Z-scored PETHs of rhythmic (D–F) and non-non-rhythmic (G–I) VP neurons aligned to cue (D and G), reward (E and H), and punishment (F and I). Data are represented as mean ± SEM.

See also Figure S7.

neurons have previously been identified as somatostatin-expressing GABAergic neurons (Espinosa et al., 2019). We found that most of these rhythmically discharging neurons showed weak or no responses to behaviorally salient events including cue tones, reward, and punishment (Figures 5C–5I; largely consistent across mice, see Figure S7). These results suggest that mostly non-bursting, non-rhythmic neurons are recruited during reinforcement learning in the VP.

Indications of multiplexed burst and single spike code in the VP

Theoretical studies have suggested that because specific biophysical mechanisms are engaged to serve burst generation, burst firing may carry a representation independent from that of single spikes, creating a specific "burst code" (Kepecs and Lisman, 2003; Kepecs et al., 2002). This may allow neurons to multiplex different sources of information; however, this idea has rarely been tested.

Therefore, we separated burst firing and single spike firing based on inter-spike interval (ISI) criteria. Specifically, bursts were defined by the first ISI <10 ms and subsequent ISIs <15 ms (Laszlovszky et al., 2020; Royer et al., 2012). Next, bursts and single spikes of each neuron were aligned to behaviorally salient events. Burst and single spike firing often carried similar information about these events, indicated by correlated peri-event time histograms (PETHs) showing similar dynamics for bursts and single spikes (Figures 6A–6C). However, a subset of bursting VP neurons showed a dissociation of burst and single spike coding. The example neuron in Figures 6D–6F (enlarged in Figure S8) increased its firing rate after cue tone presentation. However, analysis of burst and single spike occurrence revealed that whereas single spike

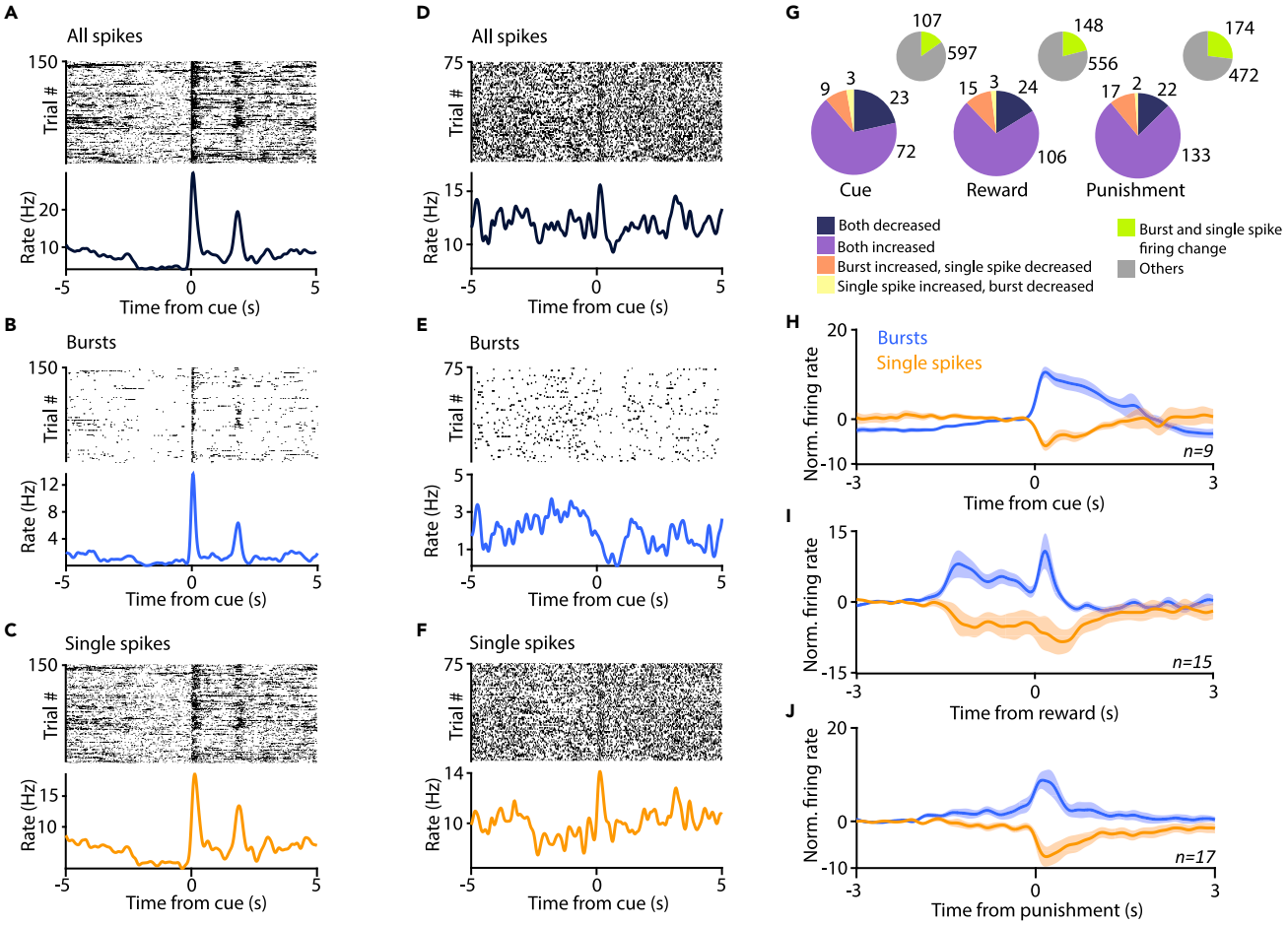

Figure 6. Dissociation of single spike and burst firing in a subset of VP neurons

(A) Example PETH of a VP neuron activated upon cue onset.

(B and C) The neuron showed increased burst (B) and single spike firing (C) after the cue.

(D–F) (D) Example of another cue-activated neuron, which showed decreased burst firing (E) and increased single spike firing (F) after cue presentation.

(G) Pie chart showing the number of neurons responding with significant rate change of both bursts and single spikes after cue (left), reward (middle), or punishment (right), pooled across mice. Insert, number of neurons where a significant change was detected for both bursts and single spikes (green).

(H–J) Average *Z*-scored PETH of burst and single spike responses of neurons where bursts showed an increase, whereas single spikes showed a decrease after cue (H), reward (I), or punishment (J). Data are represented as mean ± SEM.

See also Figure S8.

firing was elevated after the cues (Figure 6F), burst firing showed a concurrent inhibition (Figure 6E; this was not due to insufficient spike sorting). We quantified the proportion of VP neurons that showed significant opposite change of firing rate when bursts and single spikes were considered (Figures 6G-6J; opposite responses were found in 12/107, 11% of cue-responsive VP neurons; 18/148, 12% of reward-responsive VP neurons; 19/174, 11% of punishment-responsive VP neurons; for reference populations, we used the neurons where significant changes in both single spikes and bursts were found; $p < 0.01$, Mann-Whitney U test). This suggests that a subset of bursting VP neurons exhibit separate representations of external events by bursts and single spikes, revealing a distinct "burst code."

Ventral pallidal neurons form synchronously firing assemblies

Neurons in some cortical and subcortical areas have been shown to form functional assemblies of co-firing cells (Dupret et al., 2010; Fujisawa et al., 2008). We performed a cross-correlation analysis of simultaneously recorded pairs of VP neurons (n = 4,942) and found many indications of functional connectivity. Neuronal pairs often showed a zero-lag peak of cross-correlation typically taken as an indication of a common input. Narrow (1–2 ms wide) peaks within 1–4 ms from 0, on the other hand, usually indicate monosynaptic excitatory connections

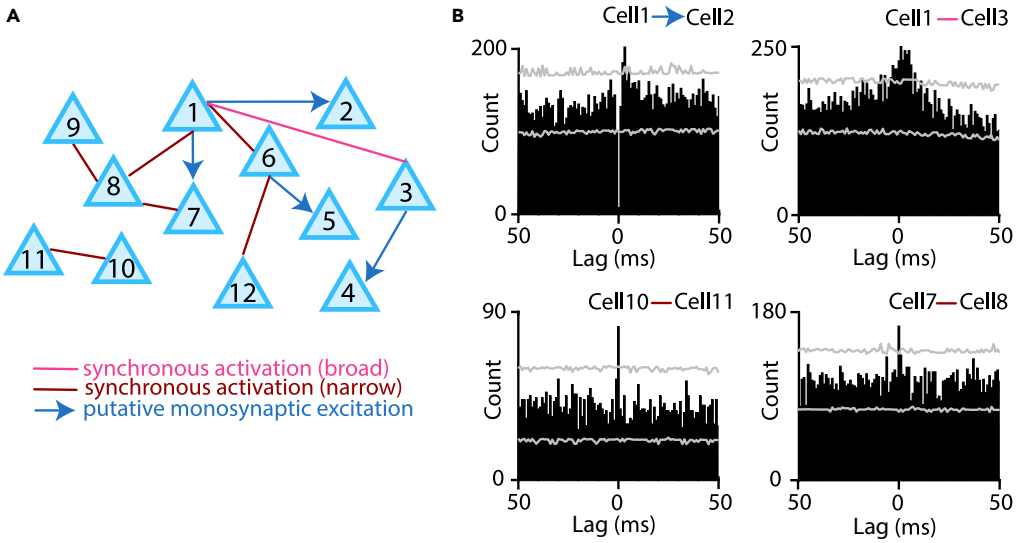

Figure 7. VP neurons form co-firing assemblies

(A) An example cell assembly formed by VP neurons during Pavlovian conditioning. Brown, narrow (1–2 ms) zero-lag synchrony; pink, broad (≥3 ms) zero-lag synchrony; blue, putative monosynaptic excitation.

(B) Example cross-correlograms of neuronal pairs of this assembly. Gray, 95% confidence intervals.

(Bartho et al., 2004; Fujisawa et al., 2008). We could identify small networks of VP neurons exhibiting pairwise synchrony, suggestive of assembly formation during associative learning in the VP (Figure 7).

Neurons participating in assemblies respond more frequently to reinforcement

VP neurons were sorted based on their cross-correlograms. Neurons that participated in synchronously firing assemblies based on significant zero-phase peaks detected in pairwise cross-correlations (Figure 7) were termed "synchronous neurons," whereas neurons wherein no such concurrent activation was observed were called "asynchronous neurons" (Figures 8A and 8B). Although this distinction probably mislabels some neurons that participate in assembly formation as "asynchronous" due to missed detections, we still uncovered prominent differences between the two groups. Neurons that participated in the detected assemblies ("synchronous group") showed higher baseline firing rates (Figure S6C) and more frequent responses to cue, reward, and punishment compared with those neurons for which we did not detect synchronous pairs ("asynchronous group"; $p = 5.64 \times 10^{-5}$, $p = 1.93 \times 10^{-8}$, $p = 6.79 \times 10^{-8}$ for cue, reward, and punishment response, respectively; chi-square test; Figures 8C–8I and S9). These differences probably represent an underestimation, because it is likely that we missed a fraction of synchronous activations.

Our results on bursting versus non-bursting, rhythmic versus non-rhythmic, and synchronous versus asynchronous neurons were not altered when neurons that potentially overlapped across recording sessions performed with small differences in dorsoventral position were excluded (n = 42/704; Figure S10; see transparent methods).

Topography of electrophysiological properties within the VP

The VP is not a homogeneous anatomical structure: based on afferent and efferent innervation patterns and marker expression, ventromedial (VPvm), dorsolateral (VPdl), ventrolateral (VPvl), and rostral (VPr) subnuclei have been described (Root et al., 2015). To differentiate ventromedial and lateral parts of the VP, we carried out triple immunostainings of choline-acetyltransferase (ChAT), neurotensin (NT), and substance P in naive mice. The area containing ChAT+ neurons and SP+ fibers marked the VP, within which the VPvm was differentiated by NT+ fibers (Figure 9A and Table 1). The immunostainings and the recording positions of electrophysiologically characterized VP neurons were aligned to a common atlas reference (Franklin and Paxinos, 2007) (see transparent methods, histology), allowing us to determine whether VP neurons were recorded from the VPvm versus lateral parts of the VP, referred to VPl hereafter. We found that the VPvm was characterized by a significantly larger fraction of bursting neurons than the VPl ($p = 7.77 \times 10^{-7}$, chi-square test), whereas no significant differences in the ratio of rhythmic versus

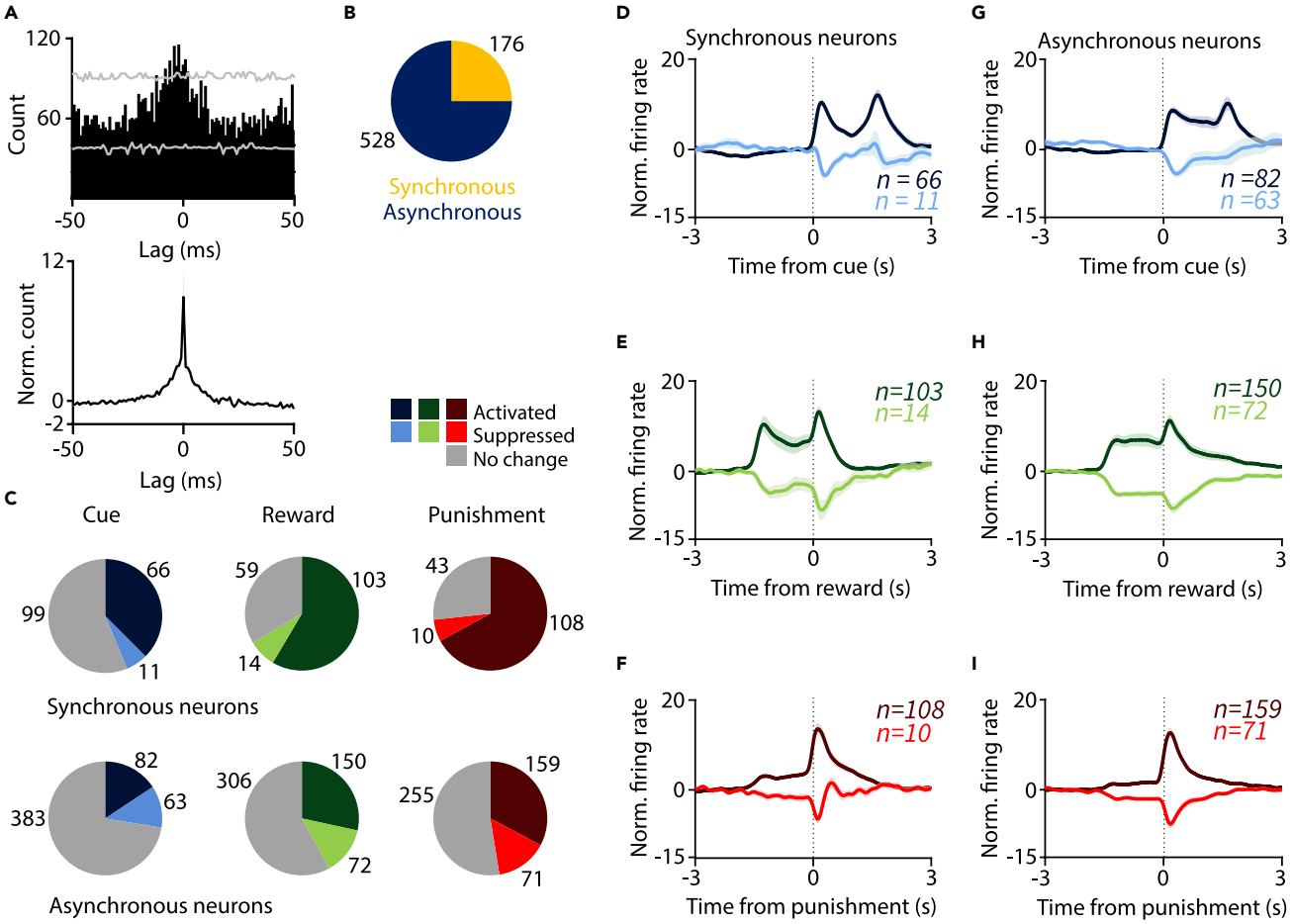

Figure 8. Synchronous neurons respond more to reinforcement

(A) Top, example cross-correlogram of synchronously activated neurons. Bottom, average cross-correlation of all synchronously active pairs.

(B) Pie chart showing the proportion of synchronous and asynchronous VP neurons, pooled across mice.

(C) Pie charts showing the number of synchronous and asynchronous VP neurons activated or inhibited by cue, reward or punishment, pooled across mice.

(D–I) Average, Z-scored PETHs of synchronous (D–F) and asynchronous (G–I) VP neurons aligned to cue (D and G), reward (E and H), and punishment (F and I). Data are represented as mean ± SEM.

See also Figure S9.

non-rhythmic and synchronous versus asynchronous neurons was detected (Figures 9B and 9C). Our observation that non-bursting, non-rhythmic VP neurons were more responsive to salient stimuli remained consistent across VPvm and VPl (Figure 9D). Finally, we discovered a dorsoventral shift in electrophysiological properties, where burst index showed a significant negative ($p = 2.93 \times 10^{-12}$) and beta rhythmicity index showed a significantly positive correlation ($p = 0.01$) with dorsoventral position, suggesting that dorsal VP neurons fire more bursts and tend to be less rhythmic compared with ventral VP (Figures 9E–9G). As most of the VPl is located ventrally to VPvm (Figure 9A), this finding is consistent with the larger proportion of burst firing neurons in VPvm.

DISCUSSION

The role of VP in reward-related and motivated behavior has been extensively studied; however, there have been very few attempts to distinguish electrophysiologically defined neuronal populations, i.e., e-types (Gouwens et al., 2019), during reinforcement learning (Avila and Lin, 2014; Kaplan et al., 2020). Therefore, the aim of this study was to characterize electrophysiologically distinct functional groups within the VP during reinforcement learning. We found that most responses to reward and punishment in the VP originated from a group of non-bursting-non-rhythmic neurons, suggesting that this population is dominant in representing reinforcers in the VP. Importantly, a subpopulation of bursting neurons showed differential

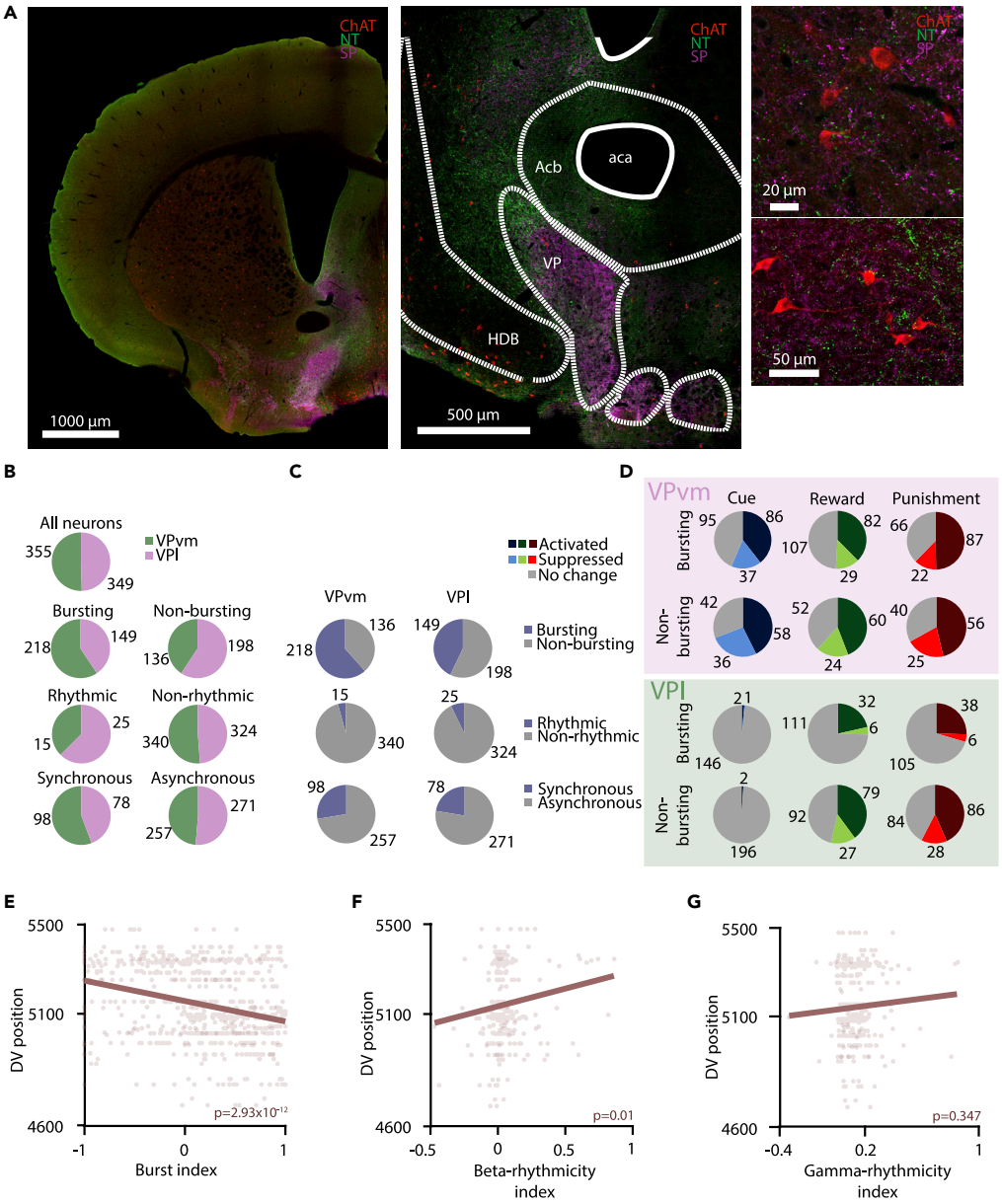

Figure 9. Comparison of ventromedial (VPvm) and lateral (VPl) subregions

(A) Fluorescent images of anti-ChAT (red), anti-NT (green), and anti-SP (magenta) triple immunohistochemical staining. Left, coronal section of a hemisphere. Scale bar, 1,000 µm. Middle, VP area. Scale bar, 500 µm. Right, high-magnification images of VP cholinergic neurons. Scale bars, 20 and 50 µm.

(B) Pie charts showing the proportion of VPvm versus VPl neurons within all recorded VP neurons and broken down to the different e-types examined.

(C) Pie charts showing the proportion of bursting versus non-bursting, rhythmic versus non-rhythmic, and synchronous versus asynchronous neurons across the VPvm and VPl subpopulations.

(D) Pie charts showing the proportion of neurons activated or suppressed after presentation of the cue, the reward, or the punishment. Bursting versus non-bursting neurons are shown for VPvm and VPl separately.

(E–G) Correlation of the burst index (E), beta-rhythmicity index (F), and gamma-rhythmicity index (G) with dorsoventral position of recorded VP neurons. Burst index showed significant negative ($p < 0.001$) and beta-rhythmicity index showed significant positive correlation ($p = 0.01$) with dorsoventral position.

responses when their bursts were contrasted with their single spikes, demonstrating that a specific "burst code" may be present in the VP (Kepecs and Lisman, 2003; Laszlovszky et al., 2020). VP neurons formed co-firing assemblies, and neurons participating in such assemblies were particularly responsive to

Table 1. Antibodies used for immunohistochemistry

Raised against	Host	Vendor	Catalog no.	Concentration
Choline acetyltransferase	Goat	Millipore	AB144P-200UL	1:500
Neurotensin	Guinea pig	Synaptic Systems	418 005	1:500
Substance P	Rabbit	Immunostar	20064	1:1000

reinforcement. We propose that electrophysiologically defined e-types of the VP differentially participate in transmitting reinforcement signals during learning.

Many studies have discussed the role of the VP in learning cue-reward associations (Ahrens et al., 2018; Avila and Lin, 2014; Fujimoto et al., 2019; Ito and Doya, 2009; Ottenheimer et al., 2018; Richard et al., 2016, 2018; Tachibana and Hikosaka, 2012; Tindell, 2004) as well as in adapting behavioral responses to outcome during reinforcement learning (e.g., "liking" reactions after reward delivery and "disgust" reactions to aversive stimuli) (Ho and Berridge, 2014; Smith and Berridge, 2005; Tindell et al., 2006), gated by internal state (Chang et al., 2017; Stephenson-Jones et al., 2020). Many of these experiments only included rewarded and omitted trials, whereas comparatively fewer articles featured aversive stimuli (Kaplan et al., 2020; Knowland et al., 2017; Saga et al., 2017; Stephenson-Jones et al., 2020; Wulff et al., 2019). Cued reward size modifications were often included (Stephenson-Jones et al., 2020; Tachibana and Hikosaka, 2012), although how the VP adapts to probabilistic cues that are notoriously harder to learn, because they require integration over many trials, has remained largely unexplored.

Therefore, we trained mice on a Pavlovian reinforcement learning task where we incorporated both reward and punishment into our task design, in order to examine VP neuronal activity patterns upon both positive and negative outcomes. We found a VP population activated by both reward and reward-predicting cues, consistent with previous findings (Ahrens et al., 2016, 2018; Stephenson-Jones et al., 2020; Tindell, 2004). However, we also found a comparable number of punishment-responsive VP neurons that have largely been overlooked before. Moreover, responses to punishment were significantly faster than reward or cue-elicited firing rate changes.

A significant population showed inhibition to cues and reinforcement regardless of valence, consistent with Type III GABAergic neurons in the study by Stephenson-Jones et al. (2020). However, we found very few neurons that responded with opposite firing rate changes to reward and punishment, unlike in the above-cited report, and in most cases the signs of responses were correlated across stimuli (Figure 2O). An important factor that likely underlies these differences is that we used a probabilistic task design, in which both cues were followed by reward, punishment, or nothing with different, set probabilities. Thus, probabilistic expectations provide a task context in which VP neurons tend to respond more positively, as all cues carry some positive value, also indicated by the dominance of neuronal activation versus inhibition in our recordings. Additionally, a number of these cells might be modulated by incentive salience rather than encoding outcome valence, as found in previous studies (Ahrens et al., 2018; Stephenson-Jones et al., 2020; Tindell, 2004; Tindell et al., 2009). We also note that most of our recordings originated from the anterior half of the VP, thus known anatomical differences along the anteroposterior axis (Mahler et al., 2014; Stratford et al., 1999) may have contributed to some of these differences.

The VP is a key node in the integration of limbic and motor processes (Fujimoto et al., 2019). The probabilistic outcome contingencies of our Pavlovian task enabled us to show that VP neurons' cue responses are modulated by reward expectation. Moreover, both the abundance of cue responses and the depth of modulation by expectation correlated with behavioral discrimination of the probabilistic cues (Stephenson-Jones et al., 2020). This finding is consistent with previous findings showing populations of VP neurons represent incentive salience (Ahrens et al., 2016, 2018; Tindell et al., 2005) or outcome prediction errors (Kaplan et al., 2020; Ottenheimer et al., 2020). The VP is known to be strongly innervated by dopaminergic fibers arising from the VTA. It appears that the functional role of this connection is the modulation of locomotion by acting on VP neuronal output (Klitenick et al., 1992). Moreover, the VTA itself is also considered to be crucial for reward expectation coding (Hollerman and Schultz, 1998) and has been shown to promote place preference via its afferent projections from the VP (Faget et al., 2018). The strong reciprocal connection between the two areas could serve as a neural basis of reward-seeking behavior in rodents. We should note, however, that the VP also lies at the intersection of basal ganglia and basal forebrain circuits, the latter

also featuring prominent reward prediction activity and salience coding (Avila and Lin, 2014; Hangya et al., 2015; Lin and Nicolelis, 2008); therefore, multiple origins of such signals are feasible. In this regard, an important finding showed that VP responses to reward appear earlier than those in the nucleus accumbens, making the previously hypothesized accumbens to VP information transfer less likely (Ottenheimer et al., 2018; Richard et al., 2016).

We characterized the activity of bursting VP neurons and found that they were less responsive to reward and punishment than non-bursting neurons. This was surprising, as bursts of action potentials are often thought to be associated with stronger excitatory drive that may lead to larger firing rate increases. Indeed, in the basal forebrain, bursting neurons as well as burst responses were associated with populations responsive to salient stimuli (Laszlovszky et al., 2020; Lin and Nicolelis, 2008). Multiple biophysical mechanisms can generate bursts of action potentials (Kim et al., 2015a; Otomo et al., 2020; Yang et al., 2018) with different temporal dynamics. We tested whether this finding was dependent on our exact burst definitions but found higher responsiveness of non-bursting neurons even when slower bursts up to 30 ms ISIs were included.

Different higher order firing patterns may represent specific information, as a special case of temporal code (Panzeri et al., 2010). Thus, bursts of action potentials conceivably code different variables from single spikes even within single neurons, allowing within-cell multiplexing of information (Kepecs and Lisman, 2003; Kepecs et al., 2002). For instance, bursts of visual thalamic neurons were shown to have sharper tuning than single spikes (Reinagel et al., 1999), and basal forebrain bursts of both cholinergic and non-cholinergic neurons represent specific information about salient stimuli (Hangya et al., 2015; Laszlovszky et al., 2020; Lin and Nicolelis, 2008). In accordance, we found VP neurons that showed strong differences in their burst and single spike occurrence after salient stimuli, which could in some cases change in opposite directions (Figure 6).

Pang and colleagues identified a fast rhythmic type of VP neuron, with rhythmicity frequency in the beta/gamma bands (Figure 8A in Pang et al., 1998). Recently, VP gamma activity was linked to somatostatin (SOM)-expressing GABAergic neurons that influenced movement speed (Espinosa et al., 2019). In contrast, SOM neurons in the medial septum did not exhibit gamma correlation. Indeed, in other parts of the basal forebrain, gamma oscillations were better correlated with parvalbumin-expressing GABAergic neurons (Kim et al., 2015b). This basal forebrain-VP dissociation posits that these SOM GABAergic VP neurons may be more linked to basal ganglia than basal forebrain activity. Consistent with this, we found that these fast-rhythmic neurons are not prominent contributors of VP reinforcement responses.

The presence of cell assemblies has previously been demonstrated in the hippocampus, nucleus accumbens, and basal forebrain (Harris et al., 2003). Dynamically forming cell assemblies of the hippocampus (Harris et al., 2003; Tingley et al., 2015; Trouche et al., 2019) were linked to spatial navigation and episodic memory recall (Dupret et al., 2010; Mamad et al., 2017; Pastalkova et al., 2008). Assemblies in the basal forebrain were suggested to organize behavior in an attention task (Tingley et al., 2014, 2015). We demonstrated that synchronously firing cell assemblies are also formed in the VP during Pavlovian conditioning. Moreover, the temporal scale of co-firing closely matched the 10–30 ms previously suggested to be a conserved parameter under biophysical constraints (Harris et al., 2003) (Figure 8A). Consistent with the idea that "transient synchrony of anatomically distributed groups of neurons underlies processing of both external sensory input and internal cognitive mechanisms" (Harris et al., 2003), we found that neurons participating in co-firing ensembles were more responsive to behaviorally important sensory signals during Pavlovian learning.

VPvm receives projections from nucleus accumbens shell and VTA neurons (Root et al., 2015). It was proposed to participate in discriminating rewarding signals, serve consummatory behavior, and participate in working memory (Jenck et al., 1986; Kalivas et al., 2001; Root et al., 2015). In contrast, VPdl receives nucleus accumbens core input and is thought to control motor output through its projections to the subthalamic nucleus (STN) and substantia nigra pars reticulata (SNr). Little is known about behavioral functions of VPvl. However, VPvm activity has also been linked to motor functions and aversion (Kitamura et al., 2001). Given that VPvm and VPdl participate in overlapping functions related to reward and punishment, it is not surprising that both VPvm and VPl neurons responded to reinforcement in the probabilistic Pavlovian task. The nucleus accumbens core-VPdl-STN/SNr route is thought to serve as an indirect motor control pathway,

relevant for movement initiation, execution, and stopping (Root et al., 2015; Tripathi et al., 2010, 2013). This strong involvement in movement control may explain the higher proportion of non-bursting neurons within the VPl, generally more sensitive to salient stimuli. Nevertheless, VP subregions are embedded in partially overlapping anatomical circuits, and better understanding of their functional distinctions will require further experiments.

The output of VP neurons can be modulated by enkephalins and dopamine, because VP neurons express μ- and κ-opioid receptors as well as D1 and D2 receptors (Clark and Bracci, 2018; Kupchik et al., 2015; Panagis et al., 1998). This receptor pattern makes the VP especially sensitive to drugs targeting the dopaminergic and opioid system, including opiates and cocaine (Creed et al., 2016; Heinsbroek et al., 2020; Mahler et al., 2014; Mickiewicz et al., 2009). A shift in the activity pattern of VP neurons can lead to maladaptive behavior, such as perseveration or intracranial self-stimulation in rodents, or severe addiction in humans (Hubner and Koob, 1990; Ottenheimer et al., 2019). Moreover, in patients with long-term addiction, the pathological function is accompanied by morphological changes (Müller et al., 2019). Therefore, the VP might be an ideal target for the treatment of drug addiction and habitual relapse. The nucleus accumbens, one of the main inputs to the VP, has already been proposed as a potential target for deep brain stimulation (DBS) in patients with addiction (Kuhn et al., 2014; Müller et al., 2015). However, the central position of the VP in the reward circuitry and its strong relation to addiction could make the VP another plausible target for DBS (Mahoney et al., 2018; Yu et al., 2016). Gaining a better foothold on understanding the activity patterns and coding schemes of the VP will be fundamental for developing an effective stimulation protocol while minimizing side effects.

Limitations of the study

In this study, we provide a comprehensive analysis of VP electrophysiologically defined cell types along several dimensions. We used a behavioral task that features the learning of probabilistic cue contingencies and both aversive and appetitive stimuli. However, the study has a number of limitations that should be addressed in future experiments. First, the potential nonspecific influence of genetic background, type of knock-in transgene, and viral injections has not been evaluated. Future studies comparing wild-type mice of different genetic background may shed light on behavioral differences across mouse strains with relevance to VP function. Second, the VP contains behaviorally relevant subdivisions of lateral VP and a small rostral nucleus (VPr), which we were unable to reliably discriminate with tetrode recordings. Optogenetic tagging of specific projection neurons by retrogradely spreading viral vectors could resolve this in the future. Third, we targeted the anterior part of the VP; therefore, potential differences between anterior and posterior locations could not be addressed. Fourth, although we attempted to discount for potential overlap in recorded neurons across recording days (see transparent methods), this lowers the sample size of independent neurons. Further subdivision of VP neurons based on either anatomical parcellation or more electrophysiological properties would require larger samples of VP neurons recorded in behaving mice.

Resource availability

Lead contact

Further information and requests for resources should be directed to and will be fulfilled by the lead contact, Balázs Hangya (hangya.balazs@koki.hu).

Materials availability

This study did not generate new unique reagents.

Data and code availability

MATLAB code developed to analyze the data presented in this study is available at www.github.com/hangyabalazs/VP_data_analysis. Electrophysiology and behavioral data are available from the lead contact upon reasonable request.

METHODS

All methods can be found in the accompanying Transparent Methods supplemental file.

SUPPLEMENTAL INFORMATION

Supplemental information can be found online at https://doi.org/10.1016/j.isci.2021.102377.

ACKNOWLEDGMENTS

We thank Katalin Lengyel for her help with histology and Katalin Sviatkó and Sergio Martínez-Bellver for their help with behavioral training. We acknowledge the help of László Barna and the Nikon Center of Excellence at the Institute of Experimental Medicine, Nikon Europe, Nikon Austria, and Auro-Science Consulting for kindly providing microscopy support. We thank Mackenzie Mathis and anonymous authors for open access science art at SciDraw (accessible at https://doi.org/10.5281/zenodo.3925907 and https://doi.org/10.5281/zenodo.3925927). This work was supported by the "Lendület" Program of the Hungarian Academy of Sciences (LP2015-2/2015), NKFIH KH125294, NKFIH K135561, and the European Research Council Starting Grant no. 715043 to B.H.; the Kerpel-Fronius Talent Support Program of Semmelweis University (EFOP-3.6.3.-VEKOP-16-2017-00009); and the New National Excellence Program of the Ministry of Innovation and Technology (ÚNKP-20-3-II) to P.H.

AUTHOR CONTRIBUTIONS

B.H. developed the idea and conceptualized the manuscript. P.H. and J.H. performed the experiments. P.H., B.H., and J.H. performed data analysis. P.H. generated the figures. B.H. and P.H. wrote the manuscript with input from J.H.

DECLARATION OF INTERESTS

The authors declare no competing financial interests.

Received: November 2, 2020
Revised: February 22, 2021
Accepted: March 26, 2021
Published: April 23, 2021

REFERENCES

Ahrens, A.M., Meyer, P.J., Ferguson, L.M., Robinson, T.E., and Wayne Aldridge, J. (2016). Neural activity in the ventral pallidum encodes variation in the incentive value of a reward cue. J. Neurosci. *36*, 7957–7970.

Ahrens, A.M., Ferguson, L.M., Robinson, T.E., and Aldridge, J.W. (2018). Dynamic encoding of incentive salience in the ventral pallidum: dependence on the form of the reward cue. ENeuro *5*, 1–16.

Ascoli, G.a, Alonso-Nanclares, L., Anderson, S.a, Barrionuevo, G., Benavides-Piccione, R., Burkhalter, A., Buzsáki, G., Cauli, B., Defelipe, J., Fairén, A., et al. (2008). Petilla terminology: nomenclature of features of GABAergic interneurons of the cerebral cortex. Nat. Rev. Neurosci. *9*, 557–568.

Avila, I., and Lin, S.-C. (2014). Distinct neuronal populations in the basal forebrain encode motivational salience and movement. Front. Behav. Neurosci. *8*, 421.

Bartho, P., Hirase, H., Monconduit, L., Zugaro, M., Harris, K.D., and Buzsaki, G. (2004). Characterization of neocortical principal cells and interneurons by network interactions and extracellular features. J. Neurophysiol. *92*, 600–608.

Chang, S.E., Smedley, E.B., Stansfield, K.J., Stott, J.J., and Smith, K.S. (2017). Optogenetic inhibition of ventral pallidum neurons impairs context-driven salt seeking. J. Neurosci. *37*, 5670–5680.

Clark, M., and Bracci, E. (2018). Dichotomous dopaminergic control of ventral pallidum neurons. Front. Cell. Neurosci. *12*, 1–19.

Creed, M., Ntamati, N.R., Chandra, R., Lobo, M.K., and Lüscher, C. (2016). Convergence of reinforcing and anhedonic cocaine effects in the ventral pallidum. Neuron *92*, 214–226.

Dupret, D., O'Neill, J., Pleydell-Bouverie, B., and Csicsvari, J. (2010). The reorganization and reactivation of hippocampal maps predict spatial memory performance. Nat. Neurosci. *13*, 995–1002.

Espinosa, N., Alonso, A., Lara-Vasquez, A., and Fuentealba, P. (2019). Basal forebrain somatostatin cells differentially regulate local gamma oscillations and functionally segregate motor and cognitive circuits. Sci. Rep. *9*, 1–12.

Faget, L., Zell, V., Souter, E., McPherson, A., Ressler, R., Gutierrez-Reed, N., Yoo, J.H., Dulcis, D., and Hnasko, T.S. (2018). Opponent control of behavioral reinforcement by inhibitory and excitatory projections from the ventral pallidum. Nat. Commun. *9*, 849.

Franklin, K.B., and Paxinos, G. (2007). The Mouse Brain in Stereotaxic Coordinates, Third Edition (Academic Press).

Fujimoto, A., Hori, Y., Nagai, Y., Kikuchi, E., Oyama, K., Suhara, T., and Minamimoto, T. (2019). Signaling incentive and drive in the primate ventral pallidum for motivational control of goal-directed action. J. Neurosci. *39*, 1793–1804.

Fujisawa, S., Amarasingham, A., Harrison, M.T., and Buzsáki, G. (2008). Behavior-dependent short-term assembly dynamics in the medial prefrontal cortex. Nat. Neurosci. *11*, 823–833.

Gouwens, N.W., Sorensen, S.A., Berg, J., Lee, C., Jarsky, T., Ting, J., Sunkin, S.M., Feng, D., Anastassiou, C.A., Barkan, E., et al. (2019). Classification of electrophysiological and morphological neuron types in the mouse visual cortex. Nat. Neurosci. *22*, 1182–1195.

Hangya, B., Ranade, S.P., Lorenc, M., and Kepecs, A. (2015). Central cholinergic neurons are rapidly recruited by reinforcement feedback. Cell *162*, 1155–1168.

Harris, K.D., Csicsvari, J., Hirase, H., Dragoi, G., and Buzsáki, G. (2003). Organization of cell assemblies in the hippocampus. Nature *424*, 552–556.

Heinsbroek, J.A., Bobadilla, A.C., Dereschewitz, E., Assali, A., Chalhoub, R.M., Cowan, C.W., and Kalivas, P.W. (2020). Opposing regulation of cocaine seeking by glutamate and GABA neurons in the ventral pallidum. Cell Rep. *30*, 2018–2027.e3.

Ho, C., and Berridge, K.C. (2014). Excessive disgust caused by brain lesions or temporary inactivations: mapping hotspots of the nucleus accumbens and ventral pallidum. Eur. J. Neurosci. *40*, 3556–3572.

Hollerman, J.R., and Schultz, W. (1998). Dopamine neurons report an error in the temporal prediction of reward during learning. Nat. Neurosci. *1*, 304–309.

Hubner, C.B., and Koob, G.F. (1990). The ventral pallidum plays a role in mediating cocaine and heroin self-administration in the rat. Brain Res. *508*, 20–29.

Ito, M., and Doya, K. (2009). Validation of decision-making models and analysis of decision variables in the rat basal ganglia. J. Neurosci. *29*, 9861–9874.

Jenck, F., Gratton, A., and Wise, R. (1986). Opposite effects of ventral tegmental and periaqueductal gray morphine injections on lateral hypothalamic stimulation-induced feeding. Brain Res. *339*, 24–32.

Kalivas, P.W., Jackson, D., Romanidies, A., Wyndham, L., and Duffy, P. (2001). Involvement of pallidothalamic circuitry in working memory. Neuroscience *104*, 129–136.

Kaplan, A., Mizrahi-Kliger, A.D., Israel, Z., Adler, A., and Bergman, H. (2020). Dissociable roles of ventral pallidum neurons in the basal ganglia reinforcement learning network. Nat. Neurosci. *23*, 556–564.

Kepecs, A., and Lisman, J. (2003). Information encoding and computation with spikes and bursts. Netw. Comput. Neural Syst. *14*, 103–118.

Kepecs, A., Wang, X.-J., and Lisman, J. (2002). Bursting neurons signal input slope. J. Neurosci. *22*, 9053–9062.

Kim, H.R., Hong, S.Z., and Fiorillo, C.D. (2015a). T-type calcium channels cause bursts of spikes in motor but not sensory thalamic neurons during mimicry of natural patterns of synaptic input. Front. Cell. Neurosci. *9*, 428.

Kim, H.R., Malik, A.N., Mikhael, J.G., Bech, P., Tsutsui-Kimura, I., Sun, F., Zhang, Y., Li, Y., Watabe-Uchida, M., Gershman, S.J., et al. (2020). A unified framework for dopamine signals across timescales. Cell *183*, 1600–1616.e25.

Kim, T., Thankachan, S., McKenna, J.T., McNally, J.M., Yang, C., Choi, J.H., Chen, L., Kocsis, B., Deisseroth, K., Strecker, R.E., et al. (2015b). Cortically projecting basal forebrain parvalbumin neurons regulate cortical gamma band oscillations. Proc. Natl. Acad. Sci. *112*, 3535–3540.

Kitamura, K., Ikeda, H., Koshikawa, N., and Cools, A. (2001). GABA(A) agents injected into the ventral pallidum differentially affect dopaminergic pivoting and cholinergic circling elicited from the shell of the nucleus accumbens. Neuroscience *104*, 117–127.

Klitenick, M.A., Deutch, A.Y., Churchill, L., and Kalivas, P.W. (1992). Topography and functional role of dopaminergic projections from the ventral mesencephalic tegmentum to the ventral pallidum. Neuroscience *50*, 371–386.

Knowland, D., Lilascharoen, V., Pacia, C.P., Shin, S., Wang, E.H.J., and Lim, B.K. (2017). Distinct ventral pallidal neural populations mediate separate symptoms of depression. Cell *170*, 284–297.e18.

Kuhn, J., Möller, M., Treppmann, J.F., Bartsch, C., Lenartz, D., Gruendler, T.O.J., Maarouf, M., Brosig, A., Barnikol, U.B., Klosterkötter, J., et al. (2014). Deep brain stimulation of the nucleus accumbens and its usefulness in severe opioid addiction. Mol. Psychiatry *19*, 145–146.

Kupchik, Y.M., Brown, R.M., Heinsbroek, J.A., Lobo, M.K., Schwartz, D.J., and Kalivas, P.W. (2015). Coding the direct/indirect pathways by D1 and D2 receptors is not valid for accumbens projections. Nat. Neurosci. *18*, 1230–1232.

Laszlovszky, T., Schlingloff, D., Hegedüs, P., Freund, T.F., Gulyás, A., Kepecs, A., and Hangya, B. (2020). Distinct synchronization, cortical coupling and behavioral function of two basal forebrain cholinergic neuron types. Nat. Neurosci. *23*, 992–1003.

Lin, S.-C., and Nicolelis, M.a L. (2008). Neuronal ensemble bursting in the basal forebrain encodes salience irrespective of valence. Neuron *59*, 138–149.

Mahler, S.V., Vazey, E.M., Beckley, J.T., Keistler, C.R., Mcglinchey, E.M., Kaufling, J., Wilson, S.P., Deisseroth, K., Woodward, J.J., and Aston-Jones, G. (2014). Designer receptors show role for ventral pallidum input to ventral tegmental area in cocaine seeking. Nat. Neurosci. *17*, 577–585.

Mahoney, E.C., Zeng, A., Yu, W., Rowe, M., Sahai, S., Feustel, P.J., Ramirez-Zamora, A., Pilitsis, J.G., and Shin, D.S. (2018). Ventral pallidum deep brain stimulation attenuates acute partial, generalized and tonic-clonic seizures in two rat models. Epilepsy Res. *142*, 36–44.

Mamad, O., Stumpp, L., McNamara, H.M., Ramakrishnan, C., Deisseroth, K., Reilly, R.B., and Tsanov, M. (2017). Place field assembly distribution encodes preferred locations. PLoS Biol. *15*, e2002365.

Maurice, N., Deniau, J.M., Menetrey, A., Glowinski, J., and Thierry, A.M. (1997). Position of the ventral pallidum in the rat prefrontal cortex-basal ganglia circuit. Neuroscience *80*, 523–534.

Mickiewicz, A.L., Dallimore, J.E., and Napier, T.C. (2009). The ventral pallidum is critically involved in the development and expression of morphine-induced sensitization. Neuropsychopharmacology *34*, 874–886.

Müller, U.J., Truebner, K., Schiltz, K., Kuhn, J., Mawrin, C., Dobrowolny, H., Bernstein, H.G., Bogerts, B., and Steiner, J. (2015). Postmortem volumetric analysis of the nucleus accumbens in male heroin addicts : implications for deep brain stimulation. Eur. Arch. Psychiatry Clin. Neurosci. *265*, 647–653.

Müller, U.J., Mawrin, C., Frodl, T., Dobrowolny, H., Busse, S., Bernstein, H.-G., Bogerts, B., Truebner, K., and Steiner, J. (2019). Reduced volumes of the external and internal globus pallidus in male heroin addicts: a postmortem study. Eur. Arch. Psychiatry Clin. Neurosci. *269*, 317–324.

Otomo, K., Perkins, J., Kulkarni, A., Stojanovic, S., Roeper, J., and Paladini, C.A. (2020). In vivo patch-clamp recordings reveal distinct subthreshold signatures and threshold dynamics of midbrain dopamine neurons. Nat. Commun. *11*, 6286.

Ottenheimer, D., Richard, J.M., and Janak, P.H. (2018). Ventral pallidum encodes relative reward value earlier and more robustly than nucleus accumbens. Nat. Commun. *9*, 4350.

Ottenheimer, D.J., Wang, K., Haimbaugh, A., Janak, P.H., and Richard, J.M. (2019). Recruitment and disruption of ventral pallidal cue encoding during alcohol seeking. Eur. J. Neurosci. *50*, 3428–3444.

Ottenheimer, D.J., Bari, B.A., Sutlief, E., Fraser, K.M., Kim, T.H., Richard, J.M., Cohen, J.Y., and Janak, P.H. (2020). A quantitative reward prediction error signal in the ventral pallidum. Nat. Neurosci. *23*, 1267–1276.

Panagis, G., Kastellakis, A., and Spyraki, C. (1998). Involvement of the ventral tegmental area opiate receptors in self-stimulation elicited from the ventral pallidum. Psychopharmacology (Berl) *139*, 222–229.

Pang, K., Tepper, J.M., and Zaborszky, L. (1998). Morphological and electrophysiological characteristics of noncholinergic basal. J. Comp. Neurol. *204*, 186–204.

Panzeri, S., Brunel, N., Logothetis, N.K., and Kayser, C. (2010). Sensory neural codes using multiplexed temporal scales. Trends Neurosci. *33*, 111–120.

Pastalkova, E., Itskov, V., Amarasingham, A., and Buzsáki, G. (2008). Internally generated cell assembly sequences in the rat hippocampus. Science *321*, 1322–1327.

Prasad, A.A., Xie, C., Chaichim, C., Nguyen, J.H., McClusky, H.E., Killcross, S., Power, J.M., and McNally, G.P. (2020). Complementary roles for ventral pallidum cell types and their projections in relapse. J. Neurosci. *40*, 880–893.

Reinagel, P., Godwin, D., Sherman, S.M., and Koch, C. (1999). Encoding of visual information by LGN bursts. J. Neurophysiol. *81*, 2558–2569.

Richard, J.M., Ambroggi, F., Janak, P.H., and Fields, H.L. (2016). Ventral pallidum neurons encode incentive value and promote cue-elicited instrumental actions. Neuron *90*, 1165–1173.

Richard, J.M., Stout, N., Acs, D., and Janak, P.H. (2018). Ventral pallidal encoding of reward-seeking behavior depends on the underlying associative structure. Elife *7*, 1–25.

Root, D.H., Melendez, R.I., Zaborszky, L., and Napier, T.C. (2015). The ventral pallidum: subregion-specific functional anatomy and roles in motivated behaviors. Prog. Neurobiol. *130*, 29–70.

Royer, S., Zemelman, B.V., Losonczy, A., Kim, J., Chance, F., Magee, J.C., and Buzsáki, G. (2012). Control of timing, rate and bursts of hippocampal place cells by dendritic and somatic inhibition. Nat. Neurosci. *15*, 769–775.

Saga, Y., Richard, A., Sgambato-Faure, V., Hoshi, E., Tobler, P.N., and Tremblay, L. (2017). Ventral

pallidum encodes contextual information and controls aversive behaviors. Cereb. Cortex *27*, 2528–2543.

Schultz, W., Dayan, P., and Montague, P.R. (1997). A neural substrate of prediction and reward. Science *275*, 1593–1599.

Smith, K.S., and Berridge, K.C. (2005). The ventral pallidum and hedonic reward: neurochemical maps of sucrose "liking" and food intake. J. Neurosci. *25*, 8637–8649.

Smith, K.S., Tindell, A.J., Aldridge, J.W., and Berridge, K.C. (2009). Ventral pallidum roles in reward and motivation. Behav. Brain Res. *196*, 155–167.

Solari, N., Sviatkó, K., Laszlovszky, T., Hegedüs, P., and Hangya, B. (2018). Open source tools for temporally controlled rodent behavior suitable for electrophysiology and optogenetic manipulations. Front. Syst. Neurosci. *12*, 18.

Stephenson-Jones, M., Bravo-Rivera, C., Ahrens, S., Furlan, A., Xiao, X., Fernandes-Henriques, C., and Li, B. (2020). Opposing contributions of GABAergic and glutamatergic ventral pallidal neurons to motivational behaviors. Neuron *105*, 921–933.e5.

Stratford, T.R., Kelley, A.E., and Simansky, K.J. (1999). Blockade of GABA(A) receptors in the medial ventral pallidum elicits feeding in satiated rats. Brain Res. *825*, 199–203.

Tachibana, Y., and Hikosaka, O. (2012). The primate ventral pallidum encodes expected reward value and regulates motor action. Neuron *76*, 826–837.

Tindell, A.J. (2004). Ventral pallidal representation of pavlovian cues and reward: population and rate codes. J. Neurosci. *24*, 1058–1069.

Tindell, A.J., Berridge, K.C., Zhang, J., Peciña, S., and Aldridge, J.W. (2005). Ventral pallidal neurons code incentive motivation: amplification by mesolimbic sensitization and amphetamine. Eur. J. Neurosci. *22*, 2617–2634.

Tindell, A.J., Smith, K.S., Peciña, S., Berridge, K.C., and Aldridge, J.W. (2006). Ventral pallidum firing codes hedonic reward: when a bad taste turns good. J. Neurophysiol. *96*, 2399–2409.

Tindell, A.J., Smith, K.S., Berridge, K.C., and Aldridge, J.W. (2009). Dynamic computation of incentive salience: "Wanting" what was never "liked. J. Neurosci. *29*, 12220–12228.

Tingley, D., Alexander, A.S., Kolbu, S., de Sa, V.R., Chiba, A.A., and Nitz, D.A. (2014). Task-phase-specific dynamics of basal forebrain neuronal ensembles. Front. Syst. Neurosci. *8*, 1–15.

Tingley, D., Alexander, A.S., Quinn, L.K., Chiba, A.A., and Nitz, D.A. (2015). Cell assemblies of the basal forebrain. J. Neurosci. *35*, 2992–3000.

Tripathi, A., Prensa, L., Cebrían, C., and Mengual, E. (2010). Axonal branching patterns of nucleus accumbens neurons in the rat. J. Comp. Neurol. *518*, 4649–4673.

Tripathi, A., Prensa, L., and Mengual, E. (2013). Axonal branching patterns of ventral pallidal neurons in the rat. Brain Struct. Funct. *218*, 1133–1157.

Trouche, S., Koren, V., Doig, N.M., Ellender, T.J., El-Gaby, M., Lopes-dos-Santos, V., Reeve, H.M., Perestenko, P.V., Garas, F.N., Magill, P.J., et al. (2019). A hippocampus-accumbens tripartite neuronal motif guides appetitive memory in space. Cell *176*, 1393–1406.e16.

de Vries, S.E.J., Lecoq, J.A., Buice, M.A., Groblewski, P.A., Ocker, G.K., Oliver, M., Feng, D., Cain, N., Ledochowitsch, P., Millman, D., et al. (2020). A large-scale standardized physiological survey reveals functional organization of the mouse visual cortex. Nat. Neurosci. *23*, 138–151.

Wulff, A.B., Tooley, J., Marconi, L.J., and Creed, M.C. (2019). Ventral pallidal modulation of aversion processing. Brain Res. *1713*, 62–69.

Yang, Y., Cui, Y., Sang, K., Dong, Y., Ni, Z., Ma, S., and Hu, H. (2018). Ketamine blocks bursting in the lateral habenula to rapidly relieve depression. Nature *554*, 317–322.

Yu, W., Walling, I., Smith, A.B., Ramirez-Zamora, A., Pilitsis, J.G., and Shin, D.S. (2016). Deep brain stimulation of the ventral pallidum attenuates epileptiform activity and seizing behavior in pilocarpine-treated rats. Brain Stimul. *9*, 285–295.

Záborszky, L., and Cullinan, W.E. (1992). Projections from the nucleus accumbens to cholinergic neurons of the ventral pallidum: a correlated light and electron microscopic double-immunolabeling study in rat. Brain Res. *570*, 92–101.

Zahm, D.S., Williams, E., and Wohltmann, C. (1996). Ventral striatopallidothalamic projection: IV. Relative involvements of neurochemically distinct subterritories in the ventral pallidum and adjacent parts of the rostroventral forebrain. J. Comp. Neurol. *364*, 340–362.

iScience, Volume *24*

Supplemental information

Differential recruitment of ventral pallidal e-types by behaviorally salient stimuli during Pavlovian conditioning

Panna Hegedüs, Julia Heckenast, and Balázs Hangya

Supplemental Figures

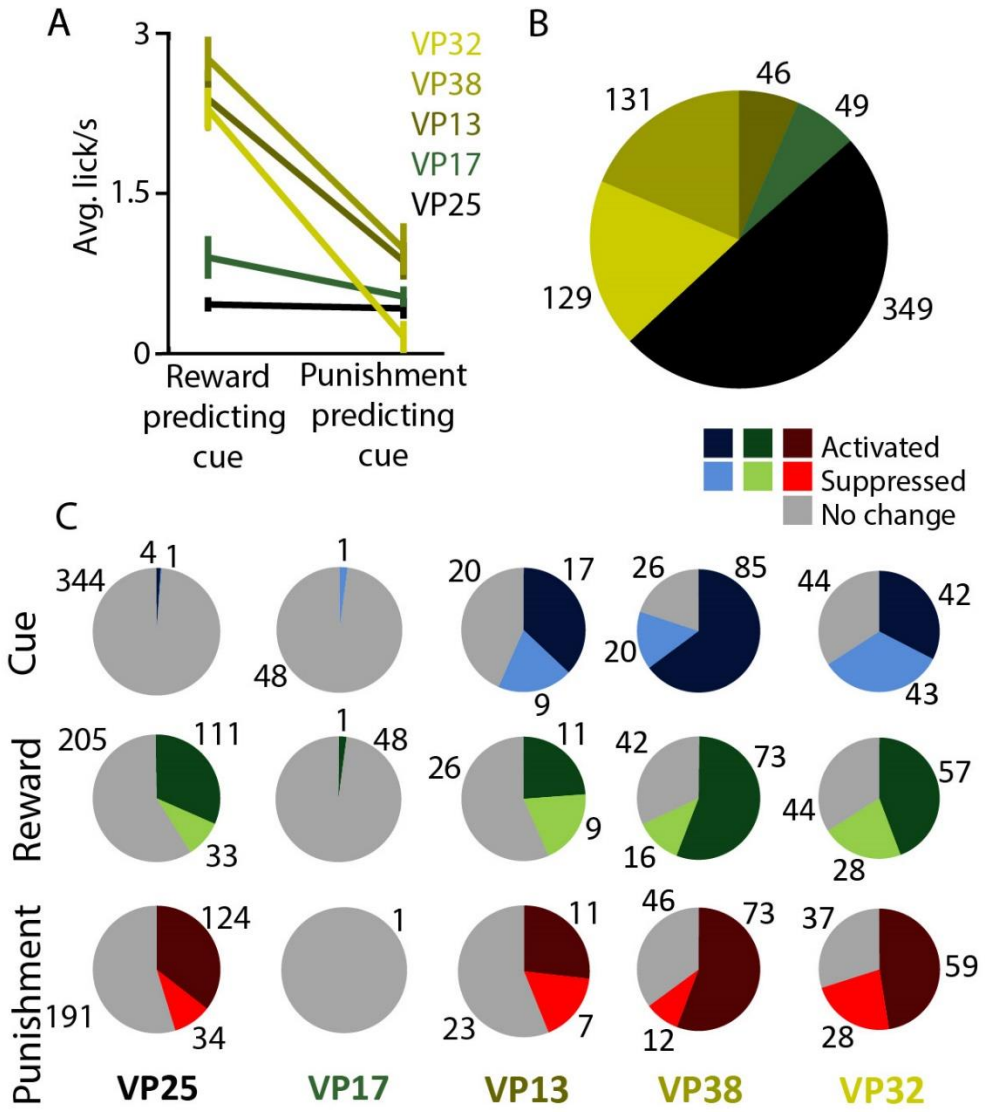

Figure S1 (Related to Figure 2). The number of cue and reinforcement responsive cells correlates with behavior. ***A,*** Line plot of anticipatory lick rate difference for reward and punishment predicting cue. Lines, corresponding to individual mice, are color coded based on anticipatory lick rate difference (yellow – large anticipatory lick rate difference, black – small anticipatory lick rate difference). Data are represented as median ± SE of median. ***B,*** Pie chart showing the number of neurons recorded in each animal (N = 5 mice). ***C,*** Pie charts showing the number of cue, reward and punishment responsive neurons in each animal.

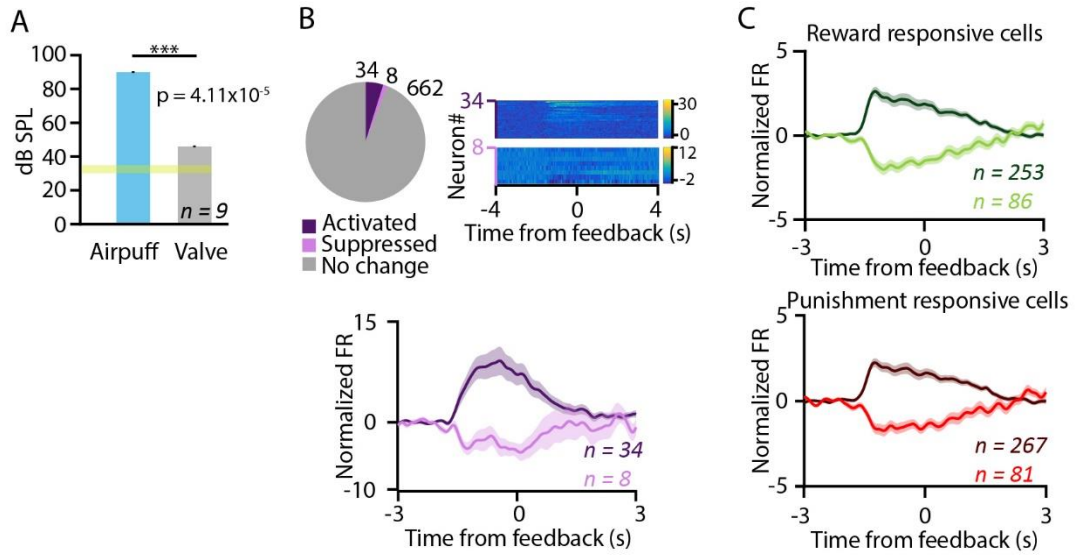

Figure S2 (Related to Figure 2). Responses to outcome omissions were rare in the VP. ***A,*** We measured the sound pressure level associated with the flow of air at air-puff punishment, the sound pressure level of the click sound of the solenoid valve at reward presentation and the ambient background noise (yellow shading). ***, $p < 0.001$, Mann-Whitney U-test. ***B,*** Pie chart showing the number of neurons that changed their firing rates significantly compared to baseline after the time point of expected but omitted reinforcement. Only few neurons showed significant firing rate differences after the time point of omitted reinforcement. These responses appeared to be better explained by the cue presentations. Data are represented as mean ± SEM. ***C,*** Peri-event time histograms of VP neurons responsive to reward or punishment, aligned to the time point of omitted reinforcers. Reward- and punishment-responsive neurons showed a smooth decay of cue-related responses at the time of omitted feedback. Data are represented as mean ± SEM.

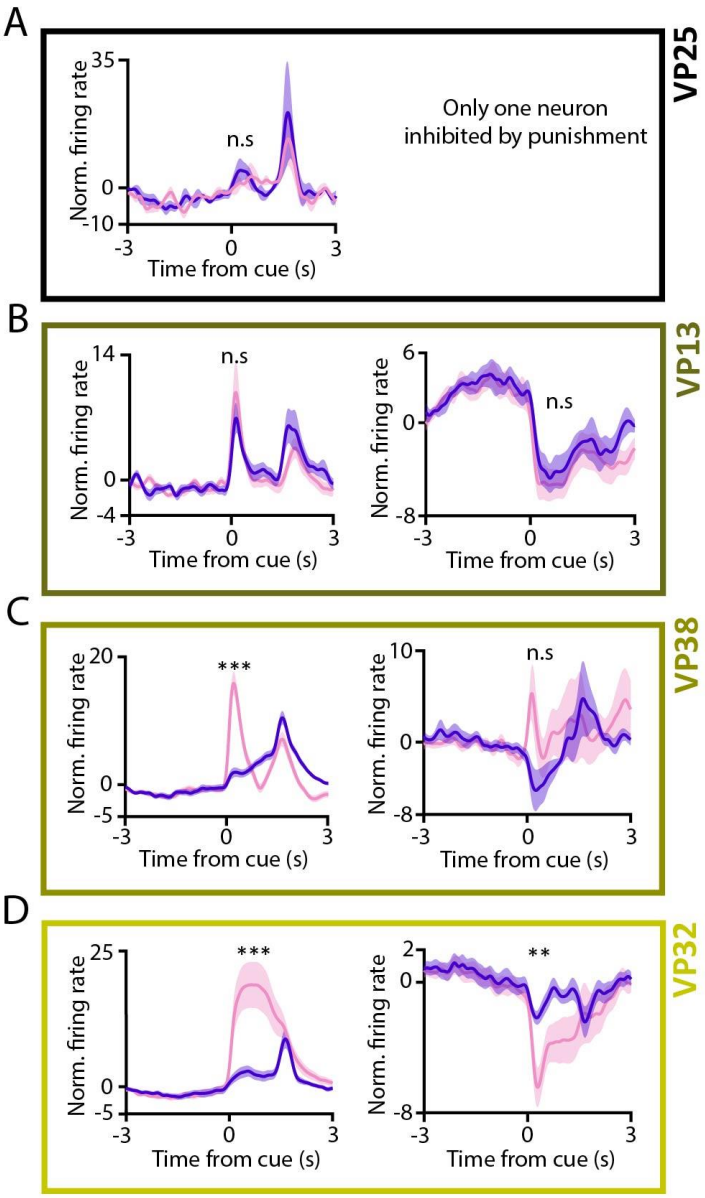

Figure S3 (Related to Figure 3). Differential neuronal response to reward and punishment predicting cues correlates with anticipatory lick difference. Average PETH of VP neuronal activation in animal VP25 ***(A)***, VP13 ***(B)***, VP38 ***(C)*** and VP32 ***(D)*** after cues predicting likely reward (pink) or likely punishment (purple). Color code corresponds to anticipatory lick rate difference (yellow – large anticipatory lick rate difference, black – small anticipatory lick rate difference). Data are represented as mean ± SEM. **, $p < 0.01$; ***, $p < 0.001$, Wilcoxon signed rank test.

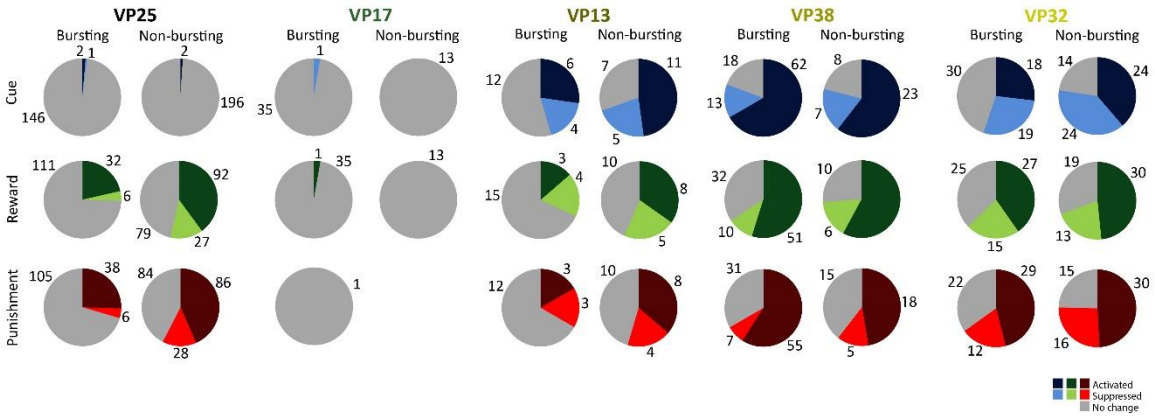

Figure S4 (Related to Figure 4). Pie charts showing the number of bursting and non-bursting cells modulated by cue, reward or punishment for individual mice. Color code of the animal corresponds to anticipatory lick rate difference (yellow – large anticipatory lick rate difference, black – small anticipatory lick rate difference).

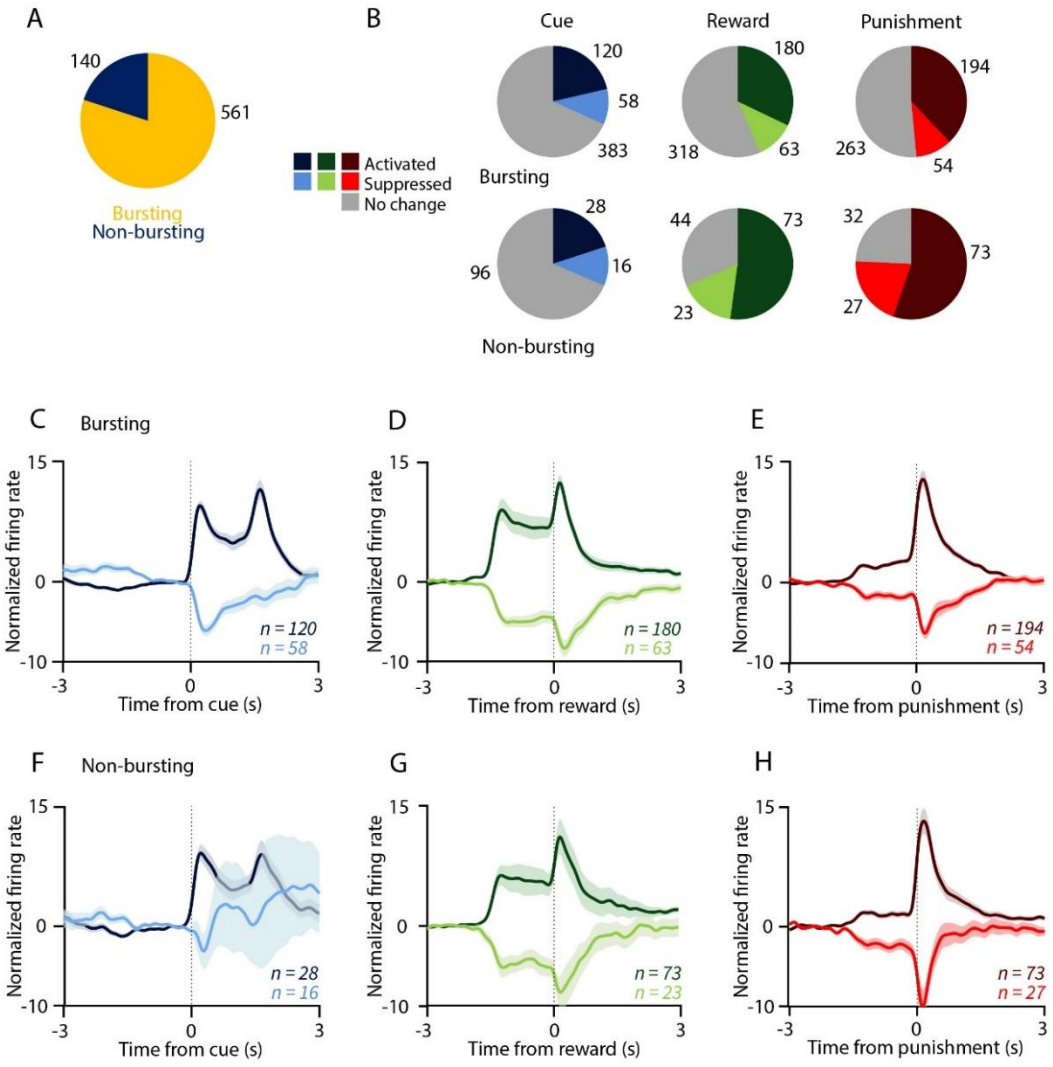

Figure S5 (Related to Figure 4). Non-bursting VP neurons respond to reinforcers more frequently, independent of ISI cutoff. ***A,*** Pie chart showing the proportion of bursting and non-bursting neurons when bursts were defined by using a 30 ms ISI cut-off. ***B,*** Pie charts showing the number of bursting and non-bursting VP neurons activated or inhibited by cue, reward or punishment. **C-H,** Average, z-scored PETHs of bursting ***(C-E)*** and non-bursting ***(F-H)*** VP neurons aligned to cue ***(C,F)*** reward ***(D,G)*** and punishment ***(E,H)***. Data are represented as mean ± SEM.

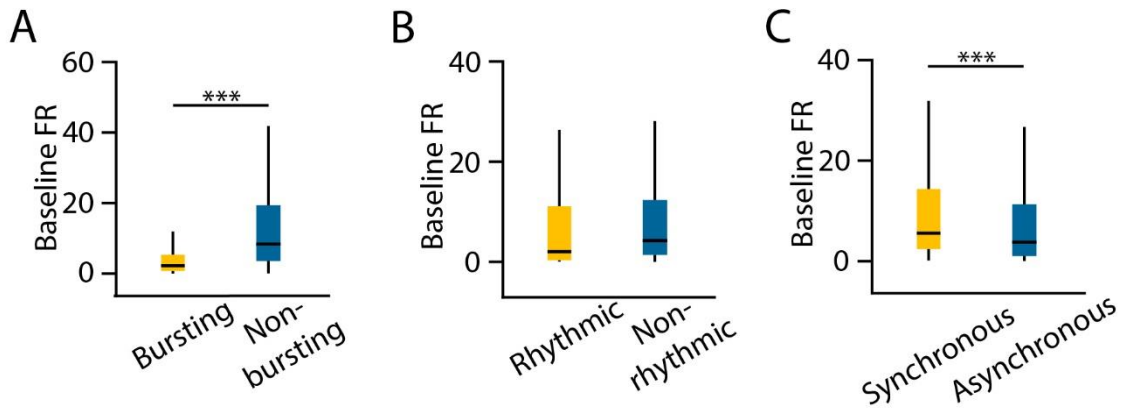

Figure S6 (Related to Figure 4). Firing rate distributions of VP e-types. ***A,*** Baseline firing rate of bursting and non-bursting neurons. ***B,*** Baseline firing rate of rhythmic and non-rhythmic neurons. ***C,*** Baseline firing rate of synchronous and asynchronous neurons. Box-whisker plots represent median, interquartile range and non-outlier range. ***, $p < 0.001$, Mann-Whitney U-test

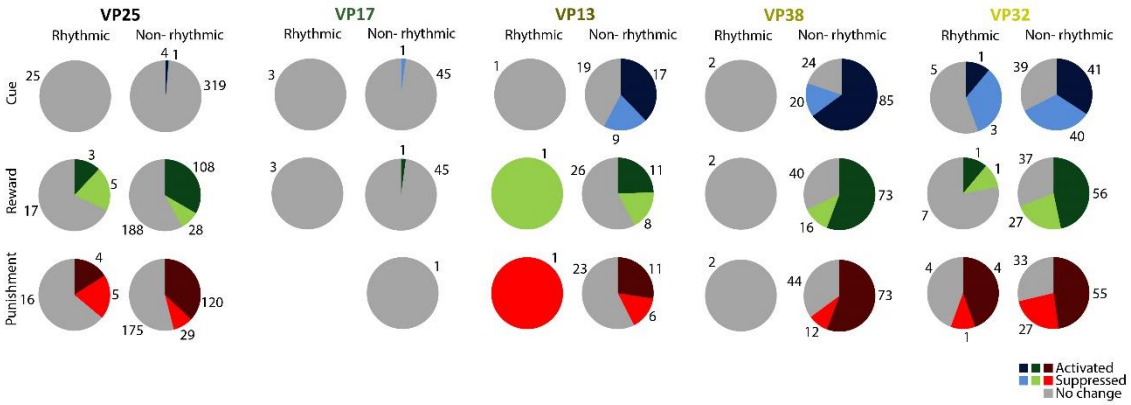

Figure S7 (Related to Figure 5). Pie charts showing the number of rhythmic and non-rhythmic neurons modulated by cue, reward or punishment for individual mice. Color code of the animal corresponds to anticipatory lick rate difference (yellow – large anticipatory lick rate difference, black – small anticipatory lick rate difference).

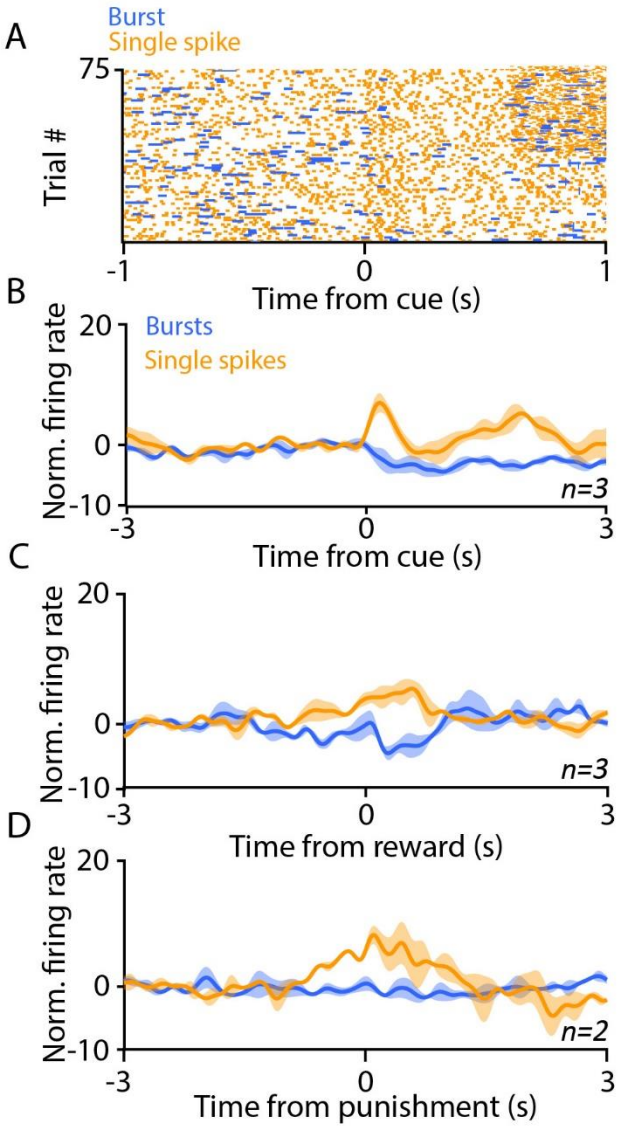

Figure S8 (Related to Figure 6). Dissociation of burst and single spike responses. ***A,*** Bursts (blue ticks) and single spikes (orange ticks) of an example neuron. Note that burst firing is decreased meanwhile single spike firing is increased upon cue presentation. ***B-D,*** Average z-scored PETH of neurons with increased single spike (orange) and decreased burst (blue) activity aligned to behaviorally salient events. Data are represented as mean ± SEM.

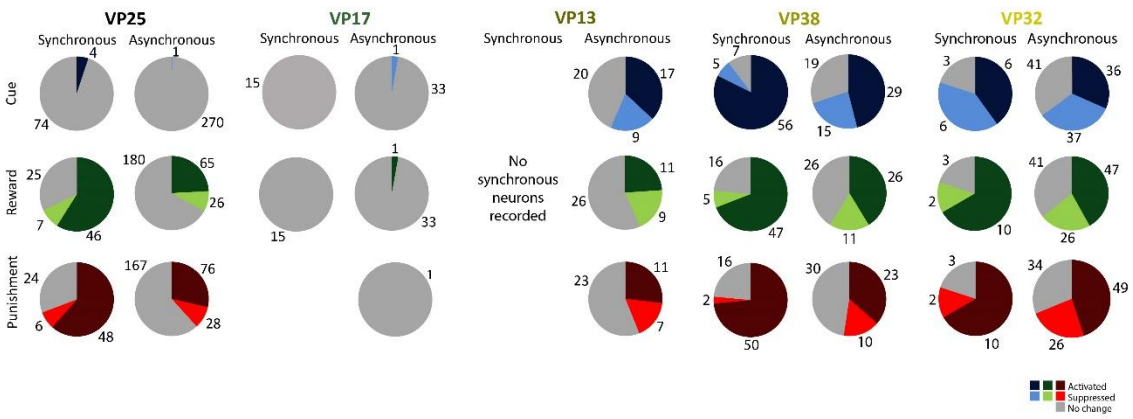

Figure S9 (Related to Figure 8). Pie charts showing the proportion of synchronous and asynchronous neurons modulated by cue, reward or punishment for individual mice. Color code of the animal corresponds to anticipatory lick rate difference (yellow – large anticipatory lick rate difference, black – small anticipatory lick rate difference).

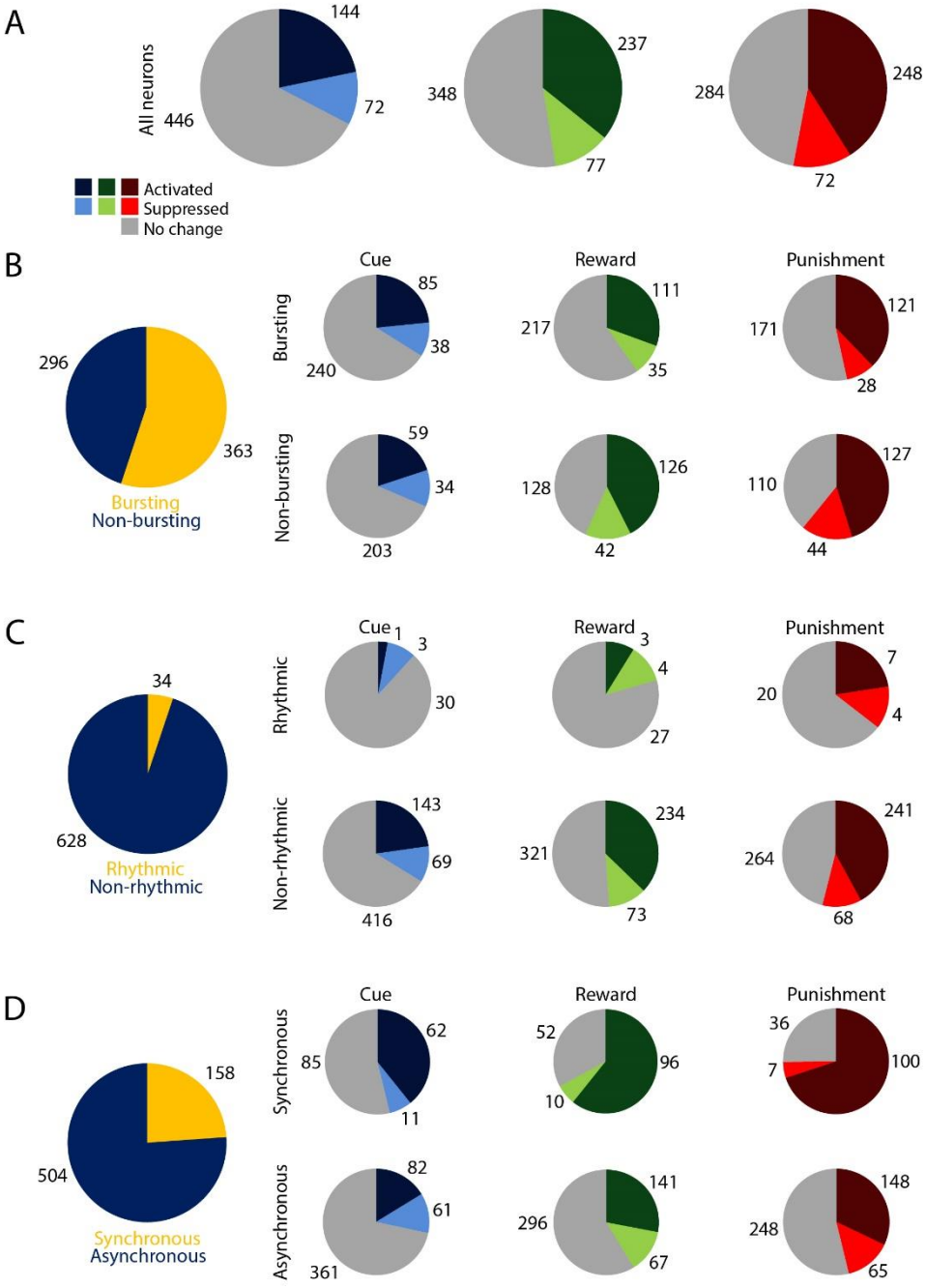

Figure S10 (Related to Figure 8). Proportion of VP e-types after potential duplicates of recorded neurons were excluded. ***A,*** Pie charts of cue, reward and punishment responsive VP cells. **B,** Left, pie chart showing the proportion of bursting and non-bursting cells. Right, pie charts showing the proportion of bursting and non-bursting VP neurons activated or inhibited by cue, reward or punishment. ***C,*** Left, pie chart showing the proportion of rhythmic and non-rhythmic cells. Right, pie charts showing the proportion of rhythmic and non- rhythmic VP neurons activated or inhibited by

cue, reward or punishment. ***D,*** Left, pie chart showing the proportion of synchronous and asynchronous cells. Right, pie charts showing the proportion of synchronous and asynchronous VP neurons activated or inhibited by cue, reward or punishment.

Transparent Methods

Animals

Adult male mice (n = 4 ChAT-IRES-Cre, B6129F1 and n = 1 PV-IRES-Cre, FVB/AntFx, VP17) were used for recording and C57Bl/6J male mice (n = 2) were used for immunohistochemistry according to the regulations of the European Community's Council Directive of November 24, 1986 (86/609/EEC). Experimental procedures were reviewed and approved by the Animal Welfare Committee of the Institute of Experimental Medicine, Budapest and by the Committee for Scientific Ethics of Animal Research of the National Food Chain Safety Office of Hungary.

Surgery

Mice were anesthetized with an intraperitoneal injection of ketamine-xylazine (0.166 and 0.006 mg/kg, respectively) after a brief induction with isoflurane. After shaving and disinfecting the scalp (Betadine), the skin was infiltrated with Lidocaine and the eyes were protected with eye ointment. Mice were placed in a stereotaxic frame and the skull was levelled along both the lateral and the antero-posterior axes. The skin, connective tissues and periosteum were removed from the skull and a cranial window was drilled above the anterior ventral pallidum (antero-posterior 0.75 mm, lateral 0.6 mm). Two additional holes were drilled above the parietal cortex for ground and reference. After virus injection to the VP (AAV 2/5. EF1a.Dio.hChR2(H134R)-eYFP.WPRE.hGH), a custom-built microdrive (Hangya et al., 2015; Kvitsiani et al., 2013) was implanted into the VP using a cannula holder on the stereotactic arm. The choice of the transgenic mouse lines and the viral construct was motivated by the prospect of optogenetic tagging (not reported). Specific expression of the fluorophore helped verifying the reconstruction of the tetrode tracks (see below). The microdrive and

a titanium headbar were secured to the skull with dental cement (LangDental acrylic powder and liquid resin, C&B Metabond quick adhesive cement). The analgesic buprenorphine (Bupaq) was administered, and mice were allowed a 1-week recovery period and handled for an additional week before training and recording.

Pavlovian cued outcome task protocol

Mice were trained on an auditory Pavlovian conditioning task in a head-fixed behavioral setup described in detail previously (Solari et al., 2018). On the first day of training, thirsty mice were head-fixed and given free access to water reward whenever they licked a waterspout. The next day, a pure tone cue was introduced that predicted likely reward. After each cue presentation, water reward was delivered with 0.8 probability with a 400-600 ms delay, while the rest of the outcomes were omissions. Next, a second pure tone cue of well-separated pitch was introduced that predicted reward with low probability (0.25). Air puff punishment (200 ms, 30 psi) was introduced in the following session with the final outcome contingencies (likely reward trials, 80% reward, 10% punishment, 10% omission; likely punishment trials, 25% reward, 65% punishment, 10% omission). The trials with different trial types (likely reward and likely punishment) and outcomes (water reward, air puff punishment and omission) were presented in a pseudorandomized order. Mice learned the task in approximately one week and consistently demonstrated reward anticipation by differential lick rate in response to the cues from the second week (Figures 1E-H).

Sound output of air-puffs and low-noise solenoid valves (LHDA0531115H, The Lee Company) were measured using a calibrated precision electret condenser microphone (EMM-6, Daytonaudio) connected to a preamplifier digital converter (AudioBox iOne, PreSonus); sound pressure levels were measured by the TrueRTA software (see (Solari et al., 2018) for more details on sounds calibration methods).

Recording

Extracellular recordings were performed with custom made microdrives consisting of 8 movable tetrode electrodes and an optical fiber. Microdirive screws were specifically designed and machined, optimized for small size and weight and having an unusually small pitch of the threading (160 µm) to allow precisely controlled descent in the brain (one eighths of a turn corresponded to 20 µm descent; M0.6 stainless steel flat head screw, 12 mm length; Easterntec, Shanghai, China). We measured the protruding length of the electrodes on each microdrive before surgery (Olympus SZ61 stereomicroscope; micro-ruler, Electron Microscopy Tools). The electrodes were dipped in DiI red fluorescent dye to aid later track reconstruction efforts.

Before each recording session, the microdrive was connected (Omnetics) to a 32-channel RHD headstage (Intan). Data were digitized at 30 kHz and transferred from the headstage to a data acquisition board (Open Ephys) via a Serial Peripheral Interface cable (Intan). The tetrodes were advanced 0-100 µm after each recording session. Throughout the experiments, detailed notes of the assumed brain coordinates during each recording session were taken based on the measured length of the tetrodes, stereotaxic information from the surgery and controlled screw turns on the microdrive.

Histology

After the *in vivo* experiments, animals were anesthetized with an intraperitoneal injection of ketamine-xylazine (0.166 and 0.006 mg/kg, respectively) and underwent an electrolytic lesioning protocol (30 µA for 5s on two leads of two selected tetrodes, which had provided high yield of recorded units; stimulator from Supertech, Pecs, Hungary). Mice were then and transcardially perfused with saline for 2 minutes and 4% para-formaldehyde (PFA) for 20 minutes. The brain was gently removed from the skull, postfixed in PFA overnight and then washed in phosphate buffer. The explanted microdrives were examined under stereomicroscope and the protruding length of the electrodes were verified against the depth registrations of the Experimenter. Coronal sections of 50 µm thickness were cut by a vibratome (Leica VT1200S). Special care was taken to section the brain

perpendicular to brain surface, so that resulting sections were in plane with coronal atlas images. The sections were washed in phosphate buffer 3 times and mounted on microscopy slides in Aquamount mounting resin. Fluorescent micrographs of the sections were taken using a Nikon C2 confocal microscope. We took 4x4 large field-of-view dark-field, red and green fluorescent images at 10x magnification.

The images taken by the confocal microscope were further processed to recover the recording location of each recording session referenced to atlas coordinates (Paxinos et al., 2001). These adjustments could account for individual size differences of mouse brains compared to the atlas reference and slight deviations from the vertical direction during electrode descent. Dark-field whole-section brain images were used for atlas alignment, since they provided the best contrast for white and grey matter structure of the brain. Atlas images of coronal sections were morphed on the corresponding dark-field brain images using Euclidean transformations only, to determine the coronal plane of the section and verify area boundaries. If the brain section was non-uniformly distorted by the fixation process, special care was taken to accurately map the vicinity of the electrode tracks within the target areas. Then, green fluorescent images of the same sections were used to verify ChAT or PV expression where appropriate. VP was characterized by intermediate ChAT expression density compared to the densely labeled HDB/MCPO and the sparse and easily distinguishable CPu. The atlas images were next superimposed on red fluorescent images of the same field-of-view, which showed the DiI-labeled electrode tracks. Coordinates of electrode entry points and deepest points in the brain marked both by small electrolytic lesions and the endpoints of DiI tracks were read. These were used to interpolate the recording locations referenced to the atlas coordinate system, based on logs of the electrode descent. Based on this localization procedure, antero-posterior, lateral and dorso-ventral coordinates as well as an atlas brain area were assigned to each recording session and thus to each recorded neuron.

Immunohistochemistry

Triple immunohistochemical staining against choline acetyltranferase (ChAT), neurotensin (NT) and substance P (SP) was carried out on 50 µm coronal sections of C57Bl/6J male mice (n = 2). After washed in 0.1M phosphate buffer (PB) and tris-buffered saline (TBS), sections were incubated in blocking medium (1% human serum albumin + 0.1% Triton-X detergent) for 1 hour. Then, sections were incubated in a mixture of primary antibodies (anti-ChAT, anti-NT and anti-SP diluted in TBS, for exact concentrations and vendors, see Table 1) at 4°C for two days. After an extensive wash in TBS, the tissue was incubated in a secondary antibody solution containing Alexa 488 conjugated donkey anti-guinea pig (1:500), Alexa 594 conjugated donkey anti-goat (1:500) and Alexa 647 conjugated donkey anti-rabbit antibodies at 4°C overnight. Finally, sections were mounted on slides in Vectashield mounting medium and images were taken with a Nikon A1R confocal microscope.

Data analysis

Data analysis was carried out using custom written Matlab code (Mathworks). Action potentials were sorted into putative single neurons manually by using MClust (A.D Redish). Only neurons with good cluster quality (isolation distance > 20 and L-ratio < 0.15) were included in the final dataset for further analysis (Hangya et al., 2015; Schmitzer-Torbert et al., 2005).

After spike sorting, the activity of individual neurons was aligned to different task events (cue presentation, reward and punishment delivery). Statistics were carried out on each neuronal unit; baseline activity was defined by taking a 1 s window before the cue, then firing rate in the baseline window was compared to firing rate in the test window (0-0.5 s after the event). The one-sided hypotheses of firing rate increase and decrease were tested by Mann-Whitney U-test ($p < 0.001$; for cue-evoked activity, separately for likely reward and likely punishment cue). Neurons were sorted into different groups based on their statistically significant responses to the behaviorally relevant events (e.g. activated by cue, inhibited by reward etc.).

Autocorrelograms (ACG) were calculated at 0.5 ms resolution. *Burst index* (BI) was calculated by the normalized difference between maximum ACG for lags 0-10 ms and mean ACG for lags 180-200 ms,

where the normalizing factor was the greater of the two numbers, yielding an index between -1 and 1 (Royer et al., 2012). A neuron with a BI > 0.2 was considered to be bursting based on empirical observation reported previously (Laszlovszky et al., 2020) and confirmed by the presence of 'burst shoulders' on average ACG in the 'bursting group' and the complete lack of 'burst shoulder' on the average ACG in the 'non-bursting' group. We confirmed that the results did not depend on the choice of the BI cut-off, as using BI > 0.4 in the definition yielded similar results. To examine burst coding in the VP, analysis of neuronal responses to reinforcement-predicting cues and reinforcers were also carried out when only bursts or single spikes were considered for a neuron. A burst was detected whenever an inter-spike interval (ISI) was < 10 ms and subsequent spikes were considered as part of the burst as long as the ISI remained < 15 ms.

Characterization of rhythmic firing in the beta-gamma range was performed based on autocorrelograms. ACG peaks were detected either in the beta (16-30Hz) or gamma (30-100 Hz) frequency range. Then, the average value of a small window (±20 ms) around the peak was compared to a value calculated from a baseline period with the same algorithm. Neurons were considered rhythmically firing when this ratio was > 0.4 for the beta and > 0.25 for the gamma band. These cut-off values were determined empirically and confirmed by observing all ACGs after sorting into rhythmicity groups.

Crosscorrelograms (CCG) were calculated at 1 ms resolution. CCGs were calculated and plotted for all simultaneously recorded pairs of neurons. Synchronously activated pairs were sorted based on a significant peak exceeding the upper 95% confidence interval by at least 10 counts of co-occurrences in the CCG around zero lag. A 1-2 ms wide asymmetric peak between 1-4 ms time lags was considered a putative monosynaptic excitatory connection based on previous reports (Bartho et al., 2004; Fujisawa et al., 2008; Hangya et al., 2010). Zero-lag synchrony was not tested for pairs of neurons recorded by the same tetrodes due to potential cluster contaminations during spike sorting.

For plotting average ACG and CCG, data were Z-score normalized with their surrogate mean and standard deviation. The surrogates were generated using the shift predictor method that introduces randomized delays between the correlated signals to generate a null distribution of no correlated activity (Fujisawa et al., 2008).

It was estimated that when extracellular electrodes are advanced in the brain, within 150 μm it is theoretically possible to capture an overlapping population of neurons (Buzsáki, 2004). There is no method to unequivocally determine whether the same neuron was being recorded by extracellular electrodes on the next day (Dhawale et al., 2017); therefore, the consensus approach is to treat every session independently. Nevertheless, to test whether potential 'duplicate' recordings introduced statistical distortions that could affect results, we adapted a method from Fraser and Schwartz (Fraser and Schwartz, 2012) to determine whether the same cell was likely captured again. This method is based on the similarity of spike shape, autocorrelation and firing rates when the same neuron is recorded across sessions. The algorithm was modified to better suite tetrode microdrive recordings as opposed to Utah and Michigan arrays, as follows. Spike waveforms were normalized to the maximum on the channel with largest amplitude. Maximum waveform crosscorrelation was calculated for pairs of neurons, so that the resulting waveform similarity scores were not sensitive to small temporal shifts (Jackson and Fetz, 2007). The waveform correlations were normalized between -1 and 1 and Fisher-transformed to yield an approximate normal distribution. We calculated spike autocorrelograms (100 ms window, 5 ms resolution), and took the Fisher-transformed Pearson's correlation coefficient. The absolute log baseline firing rate difference was used as firing rate similarity measure. Unlike Fraser and Schwartz, we did not use the crosscorrelations, because neighboring cells could easily change when the electrodes were moved, rendering crosscorrelations unreliable for scoring similarity. We obtained a bootstrap null distribution from pairs of cells recorded in different mice for the three similarity scores. We used critical values corresponding to $p = 0.05$ based on the bootstrap null distributions for pairs of neurons recorded within 150 μm distance on the same tetrode.

Since we found that moderate firing rate changes could occur between and even within recording sessions, we relaxed the critical value for baseline firing rate to $p = 0.1$.

We estimated that 42 out of 704 VP recordings could be 'duplicates' of other recorded cells. We re-ran our analyses after excluding these 42 units and found that our main results did not change (Figure S10). However, since there is no gold standard method to link neuronal identity across recording days and these methods are at best considered approximate, we did not change our original dataset.

Experimental design and statistical analyses

This study includes the analysis of 704 neurons recorded from 5 mice. These sample sizes were determined according to the standards of the field and exceed the minimal requirements of most statistical tests. However, this strategy is necessary as subsequent statistics after sorting neurons into groups have group sample sizes that are not possible to plan before conducting the experiments.

Statistical comparison of central tendencies was performed using non-parametric tests (Mann-Whitney U-test for unpaired data and Wilcoxon signed rank test for paired data) as normal distribution of the underlying data could not be determined unequivocally. Distributions over categorical variables were compared by chi square test for homogeneity. The exact p-values were reported for group comparisons.

Significant firing rate changes were evaluated at $p < 0.001$ (Mann-Whitney U-test) to keep false positive rate low. Significant activation in crosscorrelograms was determined by 95% confidence intervals generated by the shift predictor method (Fujisawa et al., 2008; Kvitsiani et al., 2013). We introduced a lower bound on effect size and required >= 10 counts above this limit to disregard very small effects, which also ensures the robustness of the bootstrap process of surrogate generation. Average auto- and crosscorrelations were calculated using Z-score normalization based on a surrogate null hypothesis distribution as described above, to allow equal weighing of individual neurons in the average.

Supplemental References

Bartho, P., Hirase, H., Monconduit, L., Zugaro, M., Harris, K.D., and Buzsaki, G. (2004). Characterization of neocortical principal cells and interneurons by network interactions and extracellular features. J. Neurophysiol. *92*, 600–608.

Buzsáki, G. (2004). Large-scale recording of neuronal ensembles. Nat. Neurosci. *7*, 446–451.

Dhawale, A.K., Poddar, R., Wolff, S.B.E., Normand, V.A., Kopelowitz, E., and Ölveczky, B.P. (2017). Automated long-term recording and analysis of neural activity in behaving animals. Elife *6*, 1–40.

Fraser, G.W., and Schwartz, A.B. (2012). Recording from the same neurons chronically in motor cortex. J. Neurophysiol. *107*, 1970–1978.

Fujisawa, S., Amarasingham, A., Harrison, M.T., and Buzsáki, G. (2008). Behavior-dependent short-term assembly dynamics in the medial prefrontal cortex. Nat. Neurosci. *11*, 823–833.

Hangya, B., Li, Y., Muller, R.U., and Czurkó, A. (2010). Complementary spatial firing in place cell-interneuron pairs. J. Physiol. *588*, 4165–4175.

Hangya, B., Ranade, S.P., Lorenc, M., and Kepecs, A. (2015). Central Cholinergic Neurons Are Rapidly Recruited by Reinforcement Feedback. Cell *162*, 1155–1168.

Jackson, A., and Fetz, E.E. (2007). Compact movable microwire array for long-term chronic unit recording in cerebral cortex of primates. J. Neurophysiol. *98*, 3109–3118.

Kvitsiani, D., Ranade, S., Hangya, B., Taniguchi, H., Huang, J.Z., and Kepecs, A. (2013). Distinct behavioural and network correlates of two interneuron types in prefrontal cortex. Nature *498*, 363–366.

Laszlovszky, T., Schlingloff, D., Hegedüs, P., Freund, T.F., Gulyás, A., Kepecs, A., and Hangya, B. (2020). Distinct synchronization, cortical coupling and behavioral function of two basal forebrain cholinergic neuron types. Nat. Neurosci. *23*, 992–1003.

Paxinos, G., Franklin, K.B.J., and Franklin, K.B.J. (2001). The mouse brain in stereotaxic coordinates (Academic Press).

Royer, S., Zemelman, B. V, Losonczy, A., Kim, J., Chance, F., Magee, J.C., and Buzsáki, G. (2012). Control of timing, rate and bursts of hippocampal place cells by dendritic and somatic inhibition. Nat. Neurosci. *15*, 769–775.

Schmitzer-Torbert, N., Jackson, J., Henze, D., Harris, K., and Redish, a D. (2005). Quantitative measures of cluster quality for use in extracellular recordings. Neuroscience *131*, 1–11.

Solari, N., Sviatkó, K., Laszlovszky, T., Hegedüs, P., and Hangya, B. (2018). Open Source Tools for Temporally Controlled Rodent Behavior Suitable for Electrophysiology and Optogenetic Manipulations. Front. Syst. Neurosci. *12*, 18.